NASA TECHNICAL MEMORANDUM

NASA TM X-52897

NASA TM X-52897

EXPERIMENTAL HEAT TRANSFER AND FLOW RESULTS FROM AN AIR-COOLED PLUG NOZZLE SYSTEM

by John S. Clark, Edwin J. Graber and David M. Straight
Lewis Research Center
Cleveland, Ohio
September, 1970

This information is being published in preliminary form in order to expedite its early release.

ABSTRACT

An air-cooled plug-type nozzle system was built and tested on an afterburning turbojet engine. Three and one-half percent of the engine primary airflow, taken from the compressor discharge ports, was used to cool the plug and supporting struts. Exhaust gas temperatures up to 3350° R (1860 K) were successfully run. Extrapolation of the wall temperature data to the average design hot gas temperature of 3500° R (1945 K) indicated that maximum wall temperatures could be maintained below about 2040° R (1133 K).

EXPERIMENTAL HEAT TRANSFER AND FLOW RESULTS FROM AN AIR-COOLED PLUG NOZZLE SYSTEM

by John S. Clark, Edwin J. Graber and David M. Straight

Lewis Research Center
Cleveland, Ohio

SUMMARY

An air-cooled plug-type nozzle system was built and tested on an afterburning turbojet engine. Three and one-half percent of the engine primary airflow, taken from the compressor discharge ports, was used to convectively cool the plug and supporting struts. Nickel fins were brazed onto the inside surface of the plug and struts to increase the heat transfer area to the coolant.

Exhaust gas temperatures as high as 3350° R (1860 K) were successfully run. The design point of 3500° R (1945 K) was not run, however, in order to maintain nozzle internal seal temperatures below about 1460° R (811 K). Extrapolation of the wall temperature data to the design point indicated that maximum wall temperatures could be maintained below about 2040° R (1133 K). The afterburner temperature profile had a cooler region in the center which eased the plug cooling air requirement.

INTRODUCTION

The Lewis Research Center has initiated a laboratory and flight research program to determine the applicability of a broad spectrum of airbreathing engine nozzles to subsonic and supersonic flight. One of the more promising of these nozzles is the plug nozzle. The plug nozzle, in addition to exhibiting high performance characteristics at both design and off-design conditions (refs. 1, 2, 3), has other advantages including lower noise levels.

Since the plug is surrounded by hot exhaust gases cooling is required during afterburning. A plug nozzle cooling system was designed at the NASA-Lewis Research Center, incorporating parallel flow convective cooling. This system was designed to maintain plug wall temperatures below 2200° R (1220 K) when subjected to 3500° R (1945 K) exhaust gases using 3½% of the engine primary air taken from the compressor discharge as the plug coolant. Since cycle efficiency is reduced when air is taken from the cycle, establishing the actual cooling requirements of the plug becomes important.

In order to determine whether or not the cooling design criteria were satisfied, a full-scale air-cooled plug nozzle was built and tested in the Propulsion Systems Laboratory (PSL) altitude chamber of the Lewis Research Center. The nozzle was installed on a J-85 afterburning turbojet engine. The J-85 engine was selected for this study because the hot gas temperatures - up to 3600° R (2000 K) - are within the range of those expected in future supersonic aircraft engines.

The nozzle throat area must be varied with the level of afterburning, and to achieve maximum thrust performance secondary shroud lengths must be varied with nozzle pressure ratio. To cover these required ranges, several fixed primary and secondary shrouds were tested. In actual application both shtrouds would be moveable, the secondary shroud would translate axially and the primary shroud would be an iris type configuration. The effect of the resulting geometries on the plug temperature distribution is discussed in this report.

The nozzle was tested over the following range of conditions. (Symbols are defined in Appendix A):

1.	Exhaust gas total pressure, P_8	1 to 3 atmos.
2.	Exhaust gas total temperature, T_8	1000° - 3350° R (1860 K)
3.	Nozzle pressure ratio, P_8/P_o	2 to 100
4.	Plug coolant flow rate, % of primary	2 to 5
5.	Throat areas	115 in^2 (742 cm^2) 140 in^2 (903 cm^2) 175 in^2 (1130 cm^2)
6.	Secondary shroud lengths, ℓ	4 in. (10.1 cm) 15 in. (38.1 cm)
7.	Engine flow rate	20 lb_m/sec (9.07 kg/sec) to 50 lb_m/sec (22.68 kg/sec)

A series of tests were run using facility cooling air and a series of tests were run in which the cooling air was obtained from the engine compressor discharge ports.

The effect of these parameters on plug wall temperature distributions are also presented in this report.

APPARATUS

Plug Nozzle

Geometries tested. - The nozzle configuration tested consisted of a 10° half-angle conical plug, truncated at 60% of the full plug length. The plug was attached to the nacelle of a J85-13GE turbojet engine upstream of the primary nozzle. The plug was 16 inches (40.6 cm) at its maximum diameter and the secondary shroud was 25 inches in diameter. The struts that support the plug were elliptical with major and minor axes of 5.5 inches (14 cm) and 2.5 inches (6.3 cm), respectively. The plug and strut assembly had a mass of about 263 pounds (119 kg) and the primary shroud had a mass of about 11 pounds (5 kg). Figure 1 shows a schematic diagram of the plug,

afterburner liner, engine nacelle, and exhaust collector as installed on the engine in the Propulsion Systems Laboratory (PSL).

A translating secondary shroud, which is required to vary the hot gas expansion ratio to maintain efficient nozzle performance over a range of nozzle pressure ratios, was simulated in these tests by a series of fixed-length shrouds. The following shroud lengths were tested:

Table I. - SECONDARY SHROUD CONFIGURATIONS

	SHROUD LENGTH	
IDENTITY	INCHES FROM ATTACHMENT CIRCLE	CM FROM ATTACHMENT CIRCLE
-111	24	61
-109	19	48
-107	16	41
-103	13	33
-101	4	10

Most of the testing was done on the longest shroud (-111) and on the (-103) shroud, however, and only the results obtained with these shrouds are discussed in this report. The ends of these two shrouds are indicated on figure 1.

Similarly, a variable-iris type primary nozzle, which is required to allow changes in engine-operating conditions (afterburner level, for example), was simulated by a series of fixed area nozzles. The primary nozzle configurations tested are summarized below:

TABLE II. - PRIMARY NOZZLE CONFIGURATIONS

	A_8		$D_{p,8}$		$D_{1,p,8}$	
	in^2	cm^2	in.	cm	in.	cm.
non-afterburning	115	742	15.5	39.4	19.6	49.8
minimum afterburning to f/a of 0.02	140	903	15.6	39.6	20.4	51.8
f/a from 0.013 to 0.044	175	1130	15.6	39.6	21.5	54.6

Cooling scheme. - The plug and strut cooling scheme is shown schematically in figure 2. Strut and plug cooling air enters the struts near the engine nacelle and makes its way radially inward toward the plug in the passage labeled "strut coolant in", on section A-A of figure 2. This passage is capped at the bottom, to prevent the coolant from dumping directly inside the plug. The coolant is forced from the "strut coolant in" passage into the "leading edge plenum" through a series of holes; from the top of the strut to the bottom there are three one-half inch (1.27 cm) diameter holes, one one-half inch (1.27 cm) by 13/16 inch (2.06 cm) oblong hole and five five-eights inch (1.59 cm) diameter holes, respectively. From the leading-edge plenum the cooling air is forced to flow through another series of holes into the finned axial coolant channels. There are thirty 0.190 inch (.492 cm) diameter holes, seventeen 0.174 inch (.442 cm) diameter holes and eight 0.094 inch (.239 cm) by 0.188 inch (0.477 cm) oblong holes in a staggered arrangement feeding the coolant channels. The axial coolant channels are formed by attaching fins (nickel 200) to the strut outer wall (Inconel 625, thickness -.062 inch (.157 cm). The fins are 1/4 inch (.635 cm) long and spaced 1/8 inch (.317 cm) apart (see section C-C of figure 2). The cooling air flows between the nickel fins around the strut to the strut trailing edge.

The flow pattern at the trailing edge is essentially the same as the leading edge, except the direction is reversed. The air passes from the coolant channels, through a staggered hole arrangement into the trailing edge plenum, through larger holes into the "strut coolant out" passage. Again the air is forced radially inward, through an opening in the strut support and into the plug cavity.

The plug cavity is closed at the plug base; the coolant is forced forward toward the plug leading edge and through a venturi-type passage where it impinges on the inside of the plug leading edge. The cooling air then enters the plug cooling channels which are made of nickel 200 fins attached to the .062 inch (.157 cm) Inconel 625 outer wall. The plug fins, shown in section B-B of figure 2, are 5/16 inch (.794 cm) long and the circumferential spacing varies, depending upon position.

Also shown on figure 2 are the plug stations 0 through 15. The number of fins between each of the plug stations is:

TABLE III - NUMBER OF FINS ALONG PLUG

Station	No. of Fins	Station	No. of Fins
0-1	6	8-9	360
1-2	6	9-10	288
2-3	72	10-11	264
3-4	144	11-12	216
4-5	192	12-13	216
5-6	240	13-14	144
6-7	336	14-15	120
7-8	360		

The number of fins, and hence, fin spacings, were selected to yield approximately uniform plug wall temperatures at the maximum heat load condition.

The inner coolant channel wall was formed by the 0.010 inch (.0254 cm) inner wall. Figure 3 shows a segment of the plug outer wall with the fins attached and the corresponding inner wall. The fins were positioned on the inside of the outer wall with a thin sheet of braze material between the fins and the outer wall. Then each fin was individually spotwelded in place. When all of the fins in the segment were in position, the unit was furnace-brazed to insure good thermal contact between the outer wall and the fins. Next, the preformed inner wall was brazed in place. The inner wall was brazed to the fins at one end to allow for differential axial thermal expansion between the inner and outer walls. Differential circumferential expansion was compensated for using bellows-type joints in the inner wall.

Figure 4 shows the plug segment with the strut attachment surfaces. The three inner pieces were welded together and attached to the three struts and are responsible for transferring the plug pressure load through the struts to the engine nacelle.

Also shown on figure 2 are the plug station 9 and 11 seals. One of these seals is shown in figure 5. A mineral wool rope-type packing was inserted beneath the retaining clips; the inner wall from the adjacent section was inserted, during assembly, between the nickel fins and the mineral wool rope. Thus it was hoped that even with relative motion caused by thermal expansion between the inner and outer walls at that point, the seal would minimize cooling air leakage from the higher pressure interior of the plug to the cooling channels. After assembly and subsequent checking, it was found that the seal permitted a rather large coolant leak at stations 9 and 11, however, and these seals had to be augmented with a high-temperature synthetic rubber sealant. The results of this attempt to stop the leaks at stations 9 and 11 are discussed in Appendix B of this report.

Figure 6 shows an assembled plug segment with some of the instrumentation installed. The standpipes shown were required to prevent shearing of the instrumentation as a result of the thermal expansion of the outer wall relative to the cooler inner wall.

Figure 7 is a photograph of the strut assembly. Nickel fins were spot-welded and furnace-brazed onto the outer wall (shown on the right in the photograph). A thin, 0.010 inch (.0254 cm), inner wall was welded onto the fins to form the coolant channels. Finally, the two halves were assembled with the inner structural assembly and the joints electron beam welded together (far left in figure 7).

When each of the plug segments and the three struts were assembled, instrumentation, which will be described in the next section, was added. All of the instrumentation leads from the plug and struts were routed through the strut coolant channels and outside the engine. Each of the plug segments were then fit together and each seam electron beam welded.

The primary nozzle was film-cooled with residual cooling from the afterburner liner, and two film-cooling slots. One of these slots was installed just upstream of the struts and the other just downstream of the struts. Secondary air also convectively cooled the primary nozzle to some extent. The secondary shroud was film-cooled with the secondary air flow. Although much film-cooling data were obtained in this series of tests, this report will be limited to the convective cooling of the struts and plug.

Eight hundred and sixty data points were taken with facility cooling air for the struts and plug and the primary nozzle film-cooling slots. This facility cooling air was approximately ambient in temperature, and the pressures and flowrates could be varied. Ninety-two data points were also taken with the cooling air obtained from the engine compressor discharge. For these tests, about $\frac{1}{2}$-$1\frac{1}{4}$ percent of the engine primary air was used to film-cool the primary nozzle. Five percent secondary air adequately cooled the secondary shroud for all the conditions tested.

Instrumentation. - The nozzle system, engine and facility were instrumented to obtain heat transfer and pressure drop data and engine thrust data. TABLE IV summarizes the types of instrumentation used.

Details of the plug thermocouples used in this study are presented in figure 8. Figure 8(a) shows a typical installation in a region of the plug where relative motion between the inner wall and the outer wall was expected. The standpipe arrangement was required to prevent the inner wall from shearing the thermocouple, or conversely, to prevent the thermocouple from damaging the thin inner wall. The thermocouples used were 0.010 inch (.0254 cm) chromel-alumel wires, swaged in 1/16 inch (.159 cm) by 0.009 inch (.023 cm) sheathing with magnesium oxide insulation. The wall thermocouple junction was formed by welding a bead on the end of each thermocouple assembly and grinding the bead flat. After continuity checks, the thermocouples were inserted in the plug wall and welded in place and finally ground flush with the outer wall surface. Finally the thermocouple was brazed to the standpipe and the standpipe brazed to the inner wall.

Many of the plug wall thermocouples did not require standpipes and they were installed as shown in figure 8(b). In this case the thermocouple sheathing was brazed directly to the plug inner wall.

A typical coolant thermocouple installation is shown in figure 8(c). The thermocouple junction was formed by spotwelding the two wires together about 1/8 inch (.317 cm) beyond the end of the sheath. A small washer was then brazed onto the thermocouple sheath and finally the thermocouple inserted through the plug inner wall and brazed in place.

Typical plug static pressure taps are illustrated in figure 9. Inconel 600 tubing 1/16 inch (.159 cm) O.D. by 0.011 inch (0.028 cm) wall was used to measure the hot gas static pressure (fig. 9(a) and 9(b)) and coolant static pressures (fig. 9(c)). The tubes were brazed to the outer plug wall and ground smooth.

TABLE IV - SUMMARY OF PLUG NOZZLE INSTRUMENTATION

COMPONENT	STATIC PRESSURES			TOTAL PRESSURES			TEMPERATURES						
	PRIMARY FLOW	SECOND-ARY FLOW	COOLANT SYSTEM	PRIMARY FLOW	SECOND-ARY FLOW	COOLANT SYSTEM	PRIMARY FLOW	SECOND-ARY FLOW	COOLANT FLOW	WALL	INNER STRUC-TURE	MISC.	TOTAL
Plug	27		29			24			40	47	9	2*	178
Struts	8		9						12	21	5		55
Primary Shroud	8	3	11						10	20			52
Secondary Shroud		9-16			4			6		4-10		1**	24-37
Cooling Air Flow-rates			21			9			4				34
Afterburner Exit Station													
Afterburning				10			2***						12
Non-afterburning	6			10			10						26
Primary Nozzle Exit Station							1***						1
Engine Operation	16			32			38					3****	80

*2 Accelerometers mounted in plug base
**1 Static Pressure on outside of secondary shroud
***Traversing water-cooled temperature probe
****2 Thrust measurements and 1 speed measurement

Figure 10 shows the coolant total pressure details. Again, Inconel 600 tubing was used. A small tube - 1/32 inch (.079 cm) O.D. by 0.005 inch (.013 cm) wall - was formed and inserted in the larger tube - .064 inch (.162 cm) by 0.011 inch (0.028 cm) wall. The small tube was brazed to the larger tube. For station 8, a small washer was brazed to the end of the larger tube and the washer brazed to the plug inner wall. At station 15, the larger tube was brazed directly to the plug base plate.

Figure 11 presents the coordinate system used to locate the plug and strut instrumentation. The distance along the plug surface, x, starts at the plug stagnation point and runs to the end of the plug, $x = L = 43.6$ inches (111 cm). Angular position is denoted by θ, starting at the top of the nozzle and increasing in a counter clockwise direction facing downstream. The three strut positions are shown in section A-A of figure 11. On the strut surface, ξ starts at the stagnation point of the strut and runs along the surface of the strut to the rear stagnation point, $\xi = \Lambda = 5.5$ inches (14 cm). Distance from the plug surface, H, begins at the plug and ends on the primary nozzle wall, $H = \eta = 6.25$ inches (15.9 cm).

Table V describes the location of each of the thermocouples and pressure taps on the plug. The instrument designations may be summarized:

First Letter:

P = Static Pressure
H = Total Pressure
T = Temperature

Second Letter:

H = Hot Gas Side (Engine Primary Gas)
C = Coolant Side
W = Heat Transfer Wall
M = Structural Material

Third and Fourth Letter:

PL = Plug
ST = Strut

Thus, TWPL-1 through TWPL-47 designate plug wall thermocouples, etc.

Much of the plug instrumentation was concentrated at two angular positions on the plug - at about 0° (in line with the top strut) and at $\theta = 60^\circ$ (between two struts). Thus, TWPL-1 through TWPL-16 were at about 0° and TWPL-17 through TWPL-31 were at about $\theta = 60^\circ$. Similarly, the plug coolant temperatures, TCPL-1 through TCPL-10 were located at about 0° and TCPL-11 through TCPL-20 were located at about 60°. Fourteen plug wall temperatures at the throat of the nozzle were also measured - TWPL-9, TWPL-24, TWPL-34, and TWPL-37 through TWPL-47. Circumferential coolant temperature distributions were measured at the nozzle throat with twelve thermocouples ($x/L = 0.3627$) and at station 15 ($x/L = 0.9909$) with twelve thermocouples.

Two rows of static pressures were measured in the coolant channels, PCPL-1 through PCPL-8 at about 0^{o}, and PCPL-9 through PCPL-16 at about 60^{o}. Also, the twelve coolant static taps at x/L = .3627 measured the circumferential static pressure distribution at the nozzle throat. Circumferential coolant total pressure surveys were made at station 15 (x/L = .9909) and at the nozzle throat (x/L = .3645).

The location of the instrumentation on the struts is presented in TABLE VI. Most of the instrumentation was concentrated on the 0^{o} strut as can be seen in Table VI.

Engine primary air flow was calculated from temperature and pressure measurements at the throat of the engine inlet bellmouth. Turbine-type flowmeters were used to measure fuel flowrates and standard orifices were used to calculate flowrates in the secondary air line, and cooling air lines during the tests using facility cooling air. During the tests in which the cooling air was obtained from the engine compressor discharge, total and static pressure taps were installed in each of the lines. After the testing was complete, each of the lines were calibrated in a flow facility and the calibration curve then included in the data reduction computer program.

J-85-13 Afterburning Turbojet Engine

The gas generator used in this study was a General Electric J85-13 afterburning turbojet engine. The engine has an eight-stage axial-flow compressor, an annular primary combustor, a two-stage axial-flow turbine, and a single circumferential V-gutter flameholder with radial spray bars in the afterburner. At standard sea level static conditions it has a rated airflow of 44 pounds per second (20 kg/sec) at a rated corrected speed of 16,500 rpm. At maximum afterburning, the engine is capable of generating gas temperatures of about $3600^{o}R$ (2000 K) at an engine pressure ratio of about 2.2.

PSL Installation

The J-85 engine was installed in the NASA Propulsion Systems Laboratory (PSL) altitude tank. A photograph of the installation is shown in figure 12. A schematic diagram of the installation is shown in figure 13. The engine stations are numbered on figure 13:

1 - engine inlet (bellmouth throat)

2 - compressor inlet

3 - compressor discharge

4 - turbine inlet

5 - turbine discharge

6 - afterburner inlet

7 - afterburner exit (nozzle inlet)

8 - primary nozzle exit

9 - ejector exit (end of secondary shroud)

10 - altitude

The engine was modified by removing its variable area nozzle, and replacing it with an instrumentation section at the afterburner exit and attaching the plug nozzle system. The engine and nozzle system was mounted from a bed plate freely suspended by four flexure rods. Pressure forces acting on the engine, nozzle and nacelle were transmitted to the load cell to measure thrust.

A small amount of air was admitted to the test section of the altitude chamber during engine operation through the bypass valves to keep the test section at an acceptable temperature level. A front bulkhead with a labyrinth seal around the throat section of the primary air bellmouth separated the engine inlet air from the exhaust and provided a means of adjusting exhaust pressure independent of inlet pressure.

Secondary nozzle airflow was measured and supplied to a toroidal manifold at the turbine discharge station to help cool the afterburner, primary nozzle and secondary shroud. Cooling air lines for the struts and plug and a small line for accelerometer cooling were brought in through the secondary shroud system and into the struts for most of the testing. Similarly, facility cooling air was measured and brought into two toroidal manifolds that fed the two film-cooling slots on the primary nozzle. For the "compressor discharge" runs, air was taken from four ports at the end of the compressor and collected in a toroidal plenum. From this plenum, three one-inch (2.54 cm) lines carried the plug and strut cooling air directly to the three struts. Similarly, three lines supplied cooling air to film-cooling slot 1 manifold and three lines carried air to film-cooling slot 2 manifold. The six lines to the film-cooling manifolds each contained small orifices to limit the flow in these lines. Accelerometer cooling air was not taken from the engine during the "compressor discharge" runs.

RESULTS AND DISCUSSION

Cooling Air Distrubutions

Summary of cooling-air leaks. - Prior to installation of the plug nozzle system in PSL, a model of the plug inner wall seals was built and leak checked. The mineral wool rope type seal was found to leak badly.

In order to do a thorough heat transfer analysis of the plug cooling channels, it was necessary to know the local flowrate in the channels as accurately as possible. Therefore, it was decided to augment the seals in an attempt to eliminate these leaks. Appendix B describes the type of seal that was used and the limitations that the use of this seal imposed upon the subsequent tests. In summary, the sealant used deteriorated when exposed to temperatures above about 1460° R (811 K); to preserve the integrity of these seals the inner wall temperatures at plug station 9 and 11 were kept below 1460° R (811 K). This temperature limit made it impossible to attain maximum afterburning with a reasonably low coolant flowrate. Appendix B also discusses a leak that existed between the strut attachment points and the plug coolant channels; the method of calibrating this leak is also discussed. Finally, Appendix B discusses a small leak that existed between the plug and the nose cap. This cap was bolted in place and air leaked in the regions between the bolts. This small leak resulted in a small amount of film cooling over the front portion of the plug. Figure 14 is a photograph of the leading edge of the plug after the testing was completed. The streaks are clearly visible where the cap leakage film-cooled the plug leading edge region.

Strut coolant distributions. - Total and static pressures were measured in each of the feedlines supplying cooling air to the three struts. Since the coolant flowrate in each of these lines is proportional to the square root of the difference between the total and static pressure, the relative amount of cooling air being supplied each strut could be compared easily. For the runs using facility cooling air, approximately 32.5 percent of the cooling air went to the 0° strut, 36.3 percent went to the 240° strut and 31.2 percent to the 120° strut. The reason these flowrates were not more nearly the same was attributed to unequal flow resistance in the lines connecting the supply to each strut. For the runs using compressor discharge air, the line lengths were practically equal and the flowrates were about 33.7, 33.9 and 32.4 percent for the 0°, 120° and 240° struts, respectively.

Coolant pressure drop as a function of flowrate. - Figure 15 presents the product of average density and static pressure drop as a function of cooling air flowrate for the struts, plugs, and struts and plug in series. The data shown for the plug and for the struts and plug is plotted as a function of the sum of the cooling air into the struts and the accelerometer cooling air. This is not strictly correct for the struts and plug in series since the accelerometer cooling air (about 0.15 pounds/second) (0.33 Kg/sec) did not flow through the strut cooling passages. The correct pressure drop can be determined from the other two lines on the figure, however. For example, at the design point, (maximum afterburning $3\frac{1}{2}\%$ coolant and sea level takeoff engine conditions), $\rho\Delta p$ for the struts and plug is 270 $lbm\text{-}lbf/ft^5$ (1.43 $Kg\text{-}N/m^5$) and 305 $lbm\text{-}lbf/ft^5$ (1.62 $Kg\text{-}N/m^5$), respectively. For a strut inlet temperature of 967° R (538 K) and estimated strut and plut outlet temperatures of 1218° R (677 K) and 2120° R (1177 K), respectively, the static pressure drops for the strut and plug are 12.8 psia (88,200 N/m^2) and 38.8 psia (267,000 N/m^2). Using the curve for the struts and plug in series yields an overall pressure drop of 49.9 psia (356,000 N/m^2) - about three percent too low.

Compressor discharge cooling air. - Although most of the test program was run with ambient facility cooling air supplied to the struts and plug cooling channels, ninety-two data points were taken with the cooling air obtained directly from the engine compressor discharge. The temperature of the compressor discharge cooling air varies with engine speed, as shown in figure 16. For 100 percent engine speed, the compressor discharge temperature averaged about 907° R (504 K). As the cooling air flows from the compressor discharge manifold to the struts, the cooling air temperature decreases since the air lines are exposed to ambient air temperatures, both outside the engine and within the secondary flow passage. The resulting cooling air temperature at the strut inlet was thus a function of the secondary flowrate and temperature, and the level of afterburning; high levels of afterburning resulted in high afterburner liner temperatures and higher radiation heat loads to the engine nacelle and cooling air lines. The resulting temperatures at the strut inlet varied between 866° R (481 K) and 904° R (502 K).

Figure 17 shows the cooling air flowrate fraction of primary flowrate as a function of primary flowrate. The figure shows that about three and one-half percent of the primary air was suppled at absolute primary flows of 21.5 lbm/sec (47.4 Kg/sec) and about 3.7 percent was supplied at primary flowrates of 44 lbm/sec (97 Kg/sec) at 100% engine speed.

Plug Pressure Distributions

Coolant axial pressure distributions. - The air coolant in the finned passages was choked at plug station 15 (the end of the plug) for all of the heat transfer runs. Thus, back pressure had no effect on coolant static pressure profiles; figure 18 shows this typical profile for four runs. As expected, most of the pressure drop occurs near the end of the plug where compressibility effects predominate.

Coolant circumferential pressure distributions. - Figure 19 compares the circumferential static-to-total pressure ratio in the coolant channels at the plug throat (station 8) and exit (station 15). Maximum and minimum Mach numbers are also indicated on the figure and imply velocity variations of approximately 25 percent at station 8 and only six percent at station 15. The position of the total probe is extremely critical at station 15 so the variation shown may be a combination of probe position and velocity variation.

Hot gas pressure distributions. - Hot gas static pressure distributions upstream of the nozzle throat were unaffected by back pressure since the nozzle was choked for all of the runs of interest. This is not the case on the supersonic side of the nozzle throat, however. Figure 20 shows the effect of nozzle pressure ratio, P_8/P_o, on the local static-to-total pressure ratio, p/P_8, as a function of distance along plug surface. The low pressure ratio cases are typical of the pressure distributions that could be expected at sea level takeoff engine conditions; the high pressure ratio case,

P_8/P_o = 11.86, is approximately fully expanded and corresponds to flight at a high altitude.

A computer program has been developed at Lewis to evaluate the performance characteristics of a fully-expanded plug-type nozzle system with secondary flow and a secondary ejector. This program was used to predict the local static pressures in the supersonic flow field for a typical fully-expanded case. Figure 21 shows the results of this program and compares these results with experimental data. The predicted values agree very well with the experimental data for both the plug surface static pressures and the ejector surface static pressures. The program was not written to evaluate static pressure distributions for pressure ratios lower than the fully-expanded cases; thus, no comparisons of this type of operation can be made.

The effect of secondary shroud length is shown in figure 22. The shroud for the square symbols was located at ℓ = 4 inches (10.1 cm); the shroud for the triangle data was located at ℓ = 15 inches (38.1 cm). For the pressure ratio shown, the pressure profiles are similar except near the end of the plug. Data for two cases with the same pressure ratio and temperature and engine absolute flow-rates of 46.3 lbm/sec (21.0 Kg/sec) and 23.65 lbm/sec (10.73 Kg/sec) indicated no effect of engine flowrate on the static pressure distribution in the supersonic stream, as expected.

Hot Gas Temperature Distributions

Station 7. - The radial variation in hot gas temperature at the afterburner exit station is shown in figure 23. These temperatures were obtained with a water-cooled traversing probe. The traces shown indicate an average of the temperatures obtained while the probe was being inserted and while it was being retracted. For non-afterburning and very low afterburner fuel flow, the variation is very small. As more fuel is burned, however, a peaked distribution develops in an annular ring - (i.e., f/a = 0.021 on figure 23). As the level of afterburning is increased, the peaked distribution remains but spreads out radially. At the fuel-air ratio of 0.039, the hot peak tended to level somewhat in the annular region but still indicated a difference from maximum temperature to centerline temperature of 960° R (533 K) - approximately 2720° R (1510 K) on the centerline and 3680° R (2045 K) maximum.

Station 8. - A traversing water-cooled probe just downstream of the primary nozzle throat yielded similar results. Figure 24 presents five of the measured profiles. Again, the measured temperatures near the plug surface (H = 0) are approximately 500° R (278 K) cooler than the maximum temperatures. These temperature profiles caused an insulating effect at the plug surface. The average hot gas temperature, $T_{8,av}$, indicated in the legend on the figure, was obtained by adding the measured turbine discharge temperature to the calibrated afterburner temperature rise. The afterburner temperature rise calibration was performed earlier on the engine with a fixed-area water-cooled nozzle.

Wall Temperatures

Effect of coolant flowrate. - Runs were made using facility cooling air during which the engine conditions (temperature, pressure, flowrate) were held constant and the cooling air flowrate was varied. Figure 25 presents the measured plug wall temperatures for two runs with flowrates of 1.874 lbm/sec (0.85 Kg/sec) and 1.525 lbm/sec (0.692 Kg/sec), respectively, and the same engine operating conditions. Similarity of the longitudinal temperature profiles for the two runs is obvious both behind (0^o location) and between (60^o location) the struts. The run with 4.3% coolant had wall temperatures about 100^o R (55 K) cooler over the entire plug surface. The decrease in wall temperature behind the struts ($x/L = .24$) was caused by the strut bypass leakage; cooling air from the strut was leaking directly into the plug cooling passages at this point. This air was cooler than the air in the plug passages; thus the wall temperatures were lower. The sharp increase in wall temperature behind the strut at $x/L = 0.37$ was probably caused by the turbulent wake behind the strut which in turn caused the cooler hot gas on the engine centerline to be mixed with the hotter primary gas of the peaked distribution previously discussed.

Effect of nozzle pressure ratio. - The large variation in local static pressure in the supersonic region for various pressure ratios was shown in figure 20. Figure 26 shows the pressure ratio effect of these variations on the plug wall temperatures. Up to and just beyond the primary nozzle throat, the wall temperatures were unaffected by pressure ratio as were the local static pressures (and, hence, local velocities). However, in the supersonic region where the local static pressures varied significantly, the wall temperatures also varied with pressure ratio. Figure 26 indicates relatively high plug wall temperatures downstream of the throat for the 3.98 pressure ratio case; these temperatures were about the same as the wall temperature at the nozzle throat. For the higher pressure ratios, these temperatures dropped off considerably; in the case of the 13.06 pressure ratio, the wall temperatures at the end of the plug were up to 300^o R (167 K) below the wall temperature at the nozzle throat.

Effect of engine flowrate. - Figure 27 presents wall temperatures as a function of distance along the plug surface for two runs with about the same pressure ratio and average total temperature. The total pressure, P_8, and engine flowrate, w_8, for the open symbols are approximately double the values for the closed symbols. Also, the shroud lengths for the two cases were different, but the effect of shroud length on wall temperature is small compared to the aforementioned effects. The wall temperatures for the higher engine flowrate case shown are approximately 70^o R (39 K) higher than the lower flowrate case over the entire plug surface. Part of this difference may be attributed to the difference in total gas temperature of 20^o R (11 K). Conversely, however, it was shown in figure 17 that more cooling air was delivered to the struts and plug for the higher flowrate cases. It is believed that the gas temperature profiles along the plug are the real cause of the wall temperature differences shown in this figure. Unfortunately gas temperature traverses

were not made for each run and this assumption cannot be verified.

Typical strut wall and coolant temperature distributions. - Figure 28 presents the results of a typical run for the strut temperatures. The hottest wall temperatures were observed at the midchord position (ξ/Λ = 0.5) for all of the runs. On another run using $3\frac{1}{2}\%$ of the compressor discharge airflow and a bulk hot gas total temperature of 3075° R (1710 K) this maximum temperature was only 1592° R (884 K) - well below the design wall temperature limit. Measured coolant temperatures are also shown on figure 28. The drop in coolant temperature at the trailing-edge of the strut at H = 4.8 inches (12.2 cm) results because the strut height decreases from leading edge to trailing edge (see fig. 7) and the fins at the top of the strut do not extend to the trailing edge. The cooler air discharging from the shorter fins mixes together and flows toward the trailing edge along a channel inside the primary nozzle. The thermocouple at ξ/Λ = 1.0 is actually within this channel and is reading an average discharge temperature.

Cooling Air Requirements

A series of runs were made using facility cooling air and with the largest primary nozzle area to determine exactly how much cooling air was required to maintain plug and strut wall temperatures below 2200° R (1220 K). Figure 29 presents plug station 8 average wall temperatures (these throat wall temperatures were the hottest temperatures on the plug surface for most of the runs) as a function of plug coolant flowrate for various hot gas total temperatures. Cross-plotting and extrapolation of this data to 3500° R (1945 K) and accounting for (1) the fact that the cooling air from the compressor discharge would be about 500° R (278 K) hotter than the facility cooling air, and (2) local hot spots, led to the estimate that $3\frac{1}{2}\%$ of the engine primary airflow - taken from the cycle at the compressor discharge - would cool the struts and plug up to gas temperatures of 3500° R (1945 K).

The compressor discharge runs were made with the cooling air lines sized to obtain about $3\frac{1}{2}$ percent of the air. Figure 30 presents plug throat wall temperatures plotted as a function of hot gas temperature for three hot gas flowrates. Again it can be seen that the higher engine flowrate conditions result in higher wall temperatures as noted on figure 27. Extrapolation of the data on figure 30 to a hot gas temperature of 3500° R (1945 K) indicates an average throat wall temperature of about 1860° R (1033 K) for the highest flowrate. Figure 31 compares the plug throat "hot spot" temperature with the average temperature; an average temperature of 1860° R (1033 K) would extrapolate to a "hot spot" of 2040° R (1133 K) - well below the 2200° R (1220 K) design temperature. Apparently the hot gas temperature profile which surrounds the plug with cooler gas is responsible for this result.

A summary plot is presented in figure 32. A run was chosen that came close to the design point for the nozzle. The design point was the sea level takeoff condition:

T_8 = 3500°R (145 K)
P_8 = 2.2 atmos.
$\dot{w}_8$ = 42.7 lbm/sec (19.4 Kg/sec)
P_8/P_o = 2.2

Wall temperatures and coolant temperatures are shown on figure 32 for engine conditions:

T_8 = 3025° R (1680 K)
P_8 = 1.78 atmos.
$\dot{w}_8$ = 41.78 lbm/sec (18.95 Kg/sec)
P_8/P_o = 3.32

Outer wall temperatures and coolant temperatures are shown in line with the 0° strut and between the 0° strut and the 120° strut. On this run, the maximum wall temperature occurred near the end of the plug rather than at the throat. Coolant temperatures and inner wall temperatures increased continuously from inlet to outlet, as expected. Two observations may be made regarding this figure. First, large circumferential wall temperature differences exist at several positions on the plug. Second, since the portion of the plug upstream of the throat is very much over-cooled, large axial temperature gradients exist.

SUMMARY OF RESULTS

The following conclusions and comments may be made from the data presented in this report.

1. It was demonstrated that a plug type nozzle could be successfully cooled with about three and one-half percent of the primary engine airflow bled from the compressor discharge with average or bulk exhaust gas temperatures as high as 3350° R (1860 K). The design hot gas temperature of 3500° R (1945 K) was not reached because of a temperature limit of 1460° R (810 K) on the nozzle internal seals. This was only a laboratory limit, however, and would not be imposed on flight hardware.

2. Extrapolation of the wall temperature data to the design hot gas temperature of 3500° R (1945 K) indicates that the average wall temperature at the throat would be about 1860° R (1030 K) using $3\frac{1}{2}$ percent coolant from the compressor discharge and hot gas conditions corresponding to a sea level takeoff engine condition. Throat "hot spot" temperature for this condition was extrapolated to 2040° R (1133 K), about 160° R (89 K) below the design value.

3. Plug wall temperatures were lower than expected because of a cool zone in the center of the afterburner temperature profile. Hot gas temperatures were as much as 500° R (278 K) cooler than maximum at a point one-half inch (1.27 cm) from the plug wall, two inches (5.08 cm) downstream of the throat.

4. Four coolant leaks were known to exist in the plug cooling channels. The two internal leaks at plug stations 9 and 11 were kept minimal by using a synthetic rubber compound to supplement the mechanical seals and maintaining the plug inner wall temperature below 1460° R (810 K). A larger internal leak existed between the strut attachment points and the plug coolant channels. The effect of this leak is apparent in the wall temperature profiles downstream of the struts. A small external leak was also found around the leading edge cap which resulted in an unknown amount of film-cooling on the outside of the plug. This leak was calibrated from the data and was found to be very small.

5. Hot gas pressure measurements on the plug surface downstream of the primary nozzle throat indicated that the local static pressure, and hence local velocity, distributions are strongly a function of nozzle pressure ratio. Furthermore, the pressure distributions are not amenable to prediction for the low pressure ratios which complicates the heat transfer analysis for these operating conditions.

REFERENCES

1. Bresnahan, Donald L.: Experimental Investigation of a 10° Conical Turbojet Plug Nozzle with Iris Primary and Translating Shroud at Mach Numbers from 0 to 2.0. NASA TM X-1709, 1968.

2. Huntley, Sidney C.; and Samanich, Nick E.: Performance of a 10° Conical Plug Nozzle Using a Turbojet Gas Generator. NASA TM X-52570, 1969.

3. Samanich, Nick E.; and Burley, Richard R.: Flight Performance of Auxiliary Inlet Ejector and Plug Nozzle at Transonic Speeds. NASA TM X-52784, 1970.

APPENDIX A - SYMBOL LIST

The following symbols, with consistent units, are used throughout this report.

A	area
D	diameter
f/a	fuel-air ratio
H	distance from plug surface
ℓ	distance downstream of nozzle throat
L	total distance along plug surface
P	total pressure
p	static pressure
r	radius
R	afterburner radius
T	temperature
$\dot{w}$	mass flowrate
x	distance along plug surface
η	maximum distance from plug to primary nozzle
θ	angle
Λ	total distance around strut surface
ρ	density
ξ	distance around strut surface

Subscripts:

av	average
c	coolant
cor	corrected
fs	film-cooling slots
in	inlet
ℓ	primary nozzle lip
L	total distance along plug surface, 43.6 in. (111 cm)
leak	leakage
M	Mach number
m	mass
max	maximum
or	orifice
o	nozzle ambient or back pressure
p	plug
pr	primary
s	secondary
T	temperature
w	wall
x	distance along plug surface
7	afterburner exit station
8	nozzle primary throat station

APPENDIX B - DETERMINATION OF COOLANT LEAKAGE RATES

The high design outer wall temperatures and resulting large thermal differential expansions between adjacent walls of the cooling passages in the air cooled plug nozzle required that a sliding seal be used in at least one direction of the three-way expansion.

Internal seals were built into the inner wall of the plug structure at plug stations 9 and 11 (fig. 2). Internal seals were also required at the joint between the three struts and the plug forward conical surface. In an effort to reduce the leakage through the metal-to-metal seal joints, mineral wool packing was inserted.

Ideally, for good heat transfer data, there should be no internal leakage from the plug interior through the seals into the coolant passages. Before engine tests began, a leakage rate calibration was made by pressurizing the plug cavity (the leading edge impingement pipe shown in figure 2 was plugged with a rubber cork). The total leakage rate through all seals, stations 9, 11 and the three strut seals, was found to be excessive as shown by the top curve in figure 33.

After evaluating several candidate materials in an oven with a fabricated seal sample, a synthetic rubber sealant was chosen. The sample data obtained with the selected material is presented in figure 34. The leakage before applying the sealant and after applying one and then a second coat is shown. Up to 600° F, no significant leakage occurred even after several hours and the material retained its resiliency. A slow deterioration of the sealant occurred above 600° F and some hardening and cracking occurred after several hours at the elevated temperatures shown.

It was decided that the sealant could be used on the plug nozzle seals, but that operation above 600° F be restricted to short duration (but long enough to get stabilized temperature data) and temperatures no higher than 1000° F.

The stations 9 and 11 seals were completely covered with a thick coating of the sealant. An attempt to seal off the strut seals was unsuccessful. The leakage shown by the bottom curve in figure 33 was therefore assumed to be the leakage through the strut seals.

During the course of the test program, it was desired to monitor the internal leakage rate for each data point taken. This was accomplished by calibrating the leading edge impingement pipe for flowrate as shown in figure 35. The cooling flow entering the struts (measured by conventional orifice flow stations), minus the flow through the impingement pipe, represents the total internal leakage flow. All internal leakage flows enter the cooling passages downstream of the impingement pipe.

The change in leakage during the course of the test program is shown in figure 36. The change in leakage was obtained by subtracting the total leakage at the beginning of the program (bottom curve of figure 33) from the total leakage when each data point was taken. The leakage history is plotted against the temperature difference between the outer and inner walls of the plug which was an indication of the amount of differential expansion existing when that point was taken. At high temperature differences the internal leakage increased markedly indicating that the seal may be opening at the high temperature differences. When lower delta T points were again run, after the high delta T points were taken, the leakage returned to low levels indicating a self-sealing quality. When the higher coolant temperature compressor discharge runs (solid symbols) were made, however, the leakage rates show more scatter and after the last few runs at sea level conditions were obtained there appeared to be evidence of a permanent increase in leakage. This was confirmed by post run total leakage test results shown in figure 33. An external leak was found to exist through the removeable nose cap which provided access to the internal impingement pipe (see figure 14). To obtain a qualitative determination of the magnitude of this leak, the flow entering the plug was compared with the flow leaving the plug (figure 37). Since the flow is choked at the coolant passage discharge, a choked flow parameter was used in figure 37 to represent the flow leaving the plug.

The data in figure 37 are separated by afterburning and non-afterburning runs. Plug wall temperatures are higher during afterburning and differential thermal expansion between the cap and the plug wall would therefore be greater. Thus, the difference between the two lines shown in figure 37 is the order of magnitude of the external leak during afterburning runs. The difference is small, however, and well within the data scatter.

TABLE V. PLUG INSTRUMENTATION (SEE FIG. 11)

Plug Wall Temperatures

	x/L	θ
TWPL-1	.0041	0°
-2	.0341	10
-3	.0536	5
-4	.1041	12.5
-5	.1352	17.5
-6	.2048	13.5
-7	.2405	1.5
-8	.2995	0
-9	.3684	0
-10	.3741	357
-11	.4273	0
-12	.5218	0
-13	.6545	0
-14	.7491	0
-15	.8705	0
-16	.9909	3.5
-17	.0341	70
-18	.0536	66
-19	.1041	65
-20	.1352	65
-21	.2048	65.5
-22	.2405	66
-23	.2995	60
-24	.3684	60
-25	.3741	59
-26	.4273	60
-27	.5218	60
-28	.6545	60
-29	.7491	60
-30	.8705	60
-31	.9909	63.5
-32	.2405	121.5
-33	.2995	120
-34	.3684	120
-35	.2405	241.5
-36	.2995	240
-37	.3684	240
-38	.3684	15
-39	.3684	45
-40	.3684	90
-41	.3684	105
-42	.3684	135
-43	.3684	150
-44	.3684	180
-45	.3684	225
-46	.3684	270
-47	.3684	315

Plug Coolant Temperatures

	x/L	θ
TCPL-1	(1)	15
-2	.0970	8.5
-3	(2)	19.5
-4	.2405	9.5
-5	.2995	3.5
-6	.3627	3.5
-7	.4259	2
-8	.5218	2
-9	.7491	13
-10	.9909	2.5
-11	(3)	75
-12	.0970	66
-13	.1711	64.5
-14	.2405	67
-15	.2995	63.5
-16	.3627	63.5
-17	.4259	62
-18	.5218	62
-19	.7491	73
-20	.9909	62.5
-21	.3627	18.5
-22	.3627	48.5
-23	.3627	93.5
-24	.3627	108.5
-25	.3627	138.5
-26	.3627	153.5
-27	.3627	183.5
-28	.3627	228.5
-29	.3627	273.5
-30	.3627	318.5
-31	.9909	20
-32	.9909	50
-33	.9909	95
-34	.9909	110
-35	.9909	140
-36	.9909	155
-37	.9909	185
-38	.9909	230
-39	.9909	275
-40	.9909	320

TABLE V. (CONTINUED) PLUG INSTRUMENTATION

Plug Inner Wall Temperatures

	x/L	θ
TMPL-1	.0950	61.5
-2	.3627	60
-3	.9909	81
-4	.1525	18
-5	.2361	8
-6	.9682	315
-7	.4045	62
-8	.4991	62
-9	.7332	73

Hot Gas Static Pressure

PHPL-1	.0000	0
-2	.1041	357.5
-3	.2939	0
-4	.3627	0
-5	.3741	14
-6	.3950	30
-7	.4273	45
-8	.4659	60
-9	.5218	75
-10	.6545	90
-11	.7491	105
-12	.8705	120
-13	.9909	131
-14	.1041	315
-15	.1352	300
-16	.2405	300
-17	.2939	270
-18	.3627	255
-19	.3741	239
-20	.3950	225
-21	.4273	210
-22	.4659	195
-23	.5218	180
-24	(4)	352.5
-25	(5)	0
-26	(6)	0
-27	.2386	358.3

Coolant Static Pressure

	x/L	θ
PCPL-1	.0511	15
-2	.0971	13.5
-3	.1568	17.5
-4	.2405	12.5
-5	.3627	11.5
-6	.5218	13
-7	.7491	3
-8	.9909	10
-9	.0511	75
-10	.0970	68.5
-11	.1711	68.5
-12	.2405	68.5
-13	.3627	71.5
-14	.5218	73
-15	.7491	63
-16	.9909	70
-17	(7)	45
-18	(8)	180
-19	(9)	5
-20	.3627	26.5
-21	.3627	56.5
-22	.3627	101.5
-23	.3627	116.5
-24	.3627	146.5
-25	.3627	161.5
-26	.3627	191.5
-27	.3627	236.5
-28	.3627	281.5
-29	.3627	326.5

TABLE V. (CONTINUED) PLUG INSTRUMENTATION

Coolant Total Pressure

	x/L	θ
HCPL-1	.9909	5
-2	.9909	22.5
-3	.9909	52.5
-4	.9909	65
-5	.9909	97.5
-6	.9909	112.5
-7	.9909	147.5
-8	.9909	157.5
-9	.9909	187.5
-10	.9909	232.5
-11	.9909	277.5
-12	.9909	322.5
-13	.3645	1.5
-14	.3645	16.5
-15	.3645	46.5
-16	.3645	61.5
-17	.3645	91.5
-18	.3645	106.5
-19	.3645	136.5
-20	.3645	151.5
-21	.3645	181.5
-22	.3645	226.5
-23	.3645	271.5
-24	.3645	316.5

(1) Impingement pipe, x/L = .0705 , R = 1: (2.54 cm)
(2) Strut bypass, x/L = .2405 , R = 6" (15.24 cm)
(3) Impingement pipe, x/L = .0705 , R = 1" (2.54 cm)
(4) Plug Base , x/L = 1.000 , R = 2.54" (6.45 cm)
(5) Plug Base , x/L = 1.000, R = 1.25 (3.18 cm)
(6) Plug Base , x/L = 1.000 , R = 0 (0 cm)
(7) Impingement pipe, x/L = .0705 , R = 1" (2.54 cm)
(8) Inside Plug , x/L = .2700
(9) Inside Plug , x/L = .2700

TABLE VI. STRUT INSTRUMENTATION (SEE FIG. 11)

Strut Wall Temperatures

	ξ/Λ	H/η	θ
TWST-1	.0000	.13760	0°
-2	.1818	.13760	0
-3	.4636	.13760	0
-4	.7636	.13760	0
-5	.1564	.13760	0
-6	.0000	.45760	0
-7	.1818	.45760	0
-8	.4636	.45760	0
-9	.7636	.45760	0
-10	1.0000	.45760	0
-11	.0000	.73760	0
-12	.1818	.73760	0
-13	.4636	.73760	0
-14	.7636	.73760	0
-15	1.0000	.73760	0
-16	.0000	.45760	120°
-17	.4636	.45760	120°
-18	1.0000	.45760	120
-19	.0000	.45760	240
-20	.4636	.45760	240
-21	1.0000	.45760	240

Strut Coolant Temperatures

	ξ/Λ	H/η	θ
TCST-1	.2818	.10720	0°
-2	.7182	.10720	0
-3	.9091	.10720	0
-4	.2818	.42720	0
-5	.7182	.42720	0
-6	.9091	.42720	0
-7	.2818	.76800	0
-8	.7182	.76800	0
-9	.6364	.96000	0
-10	.9091	.42720	0
-11	.9091	.42720	0
-12	.0909	.08800	0

Strut Inner Wall Temperatures

	ξ/Λ	H/h	θ
TMST-1	.0455	.42720	0°
-2	.4091	.42720	0
-3	.9455	.42720	0
-4	.4091	.26720	0
-5	.4091	.70880	0

Hot Gas Static Pressure

	ξ/Λ	H/h	θ
PHST-1	.0000	.51840	0°
-2	.2000	.51840	0
-3	.4636	.51840	0
-4	.7636	.51840	0
-5	.5891	.88000	0
-6	.5891	.40800	0
-7	.2255	.40800	120
-3	.9073	.40800	120

Coolant Static Pressure

	ξ/Λ	H/h	θ
PCST-1	.0455	.16800	0°
-2	.4636	.16800	0
-3	.9545	.16800	0
-4	.0455	.48800	0
-5	.4636	.48800	0
-6	.9545	.48800	0
-7	.0455	.76800	0
-8	.4636	.76800	0
-9	.6364	.96000	0

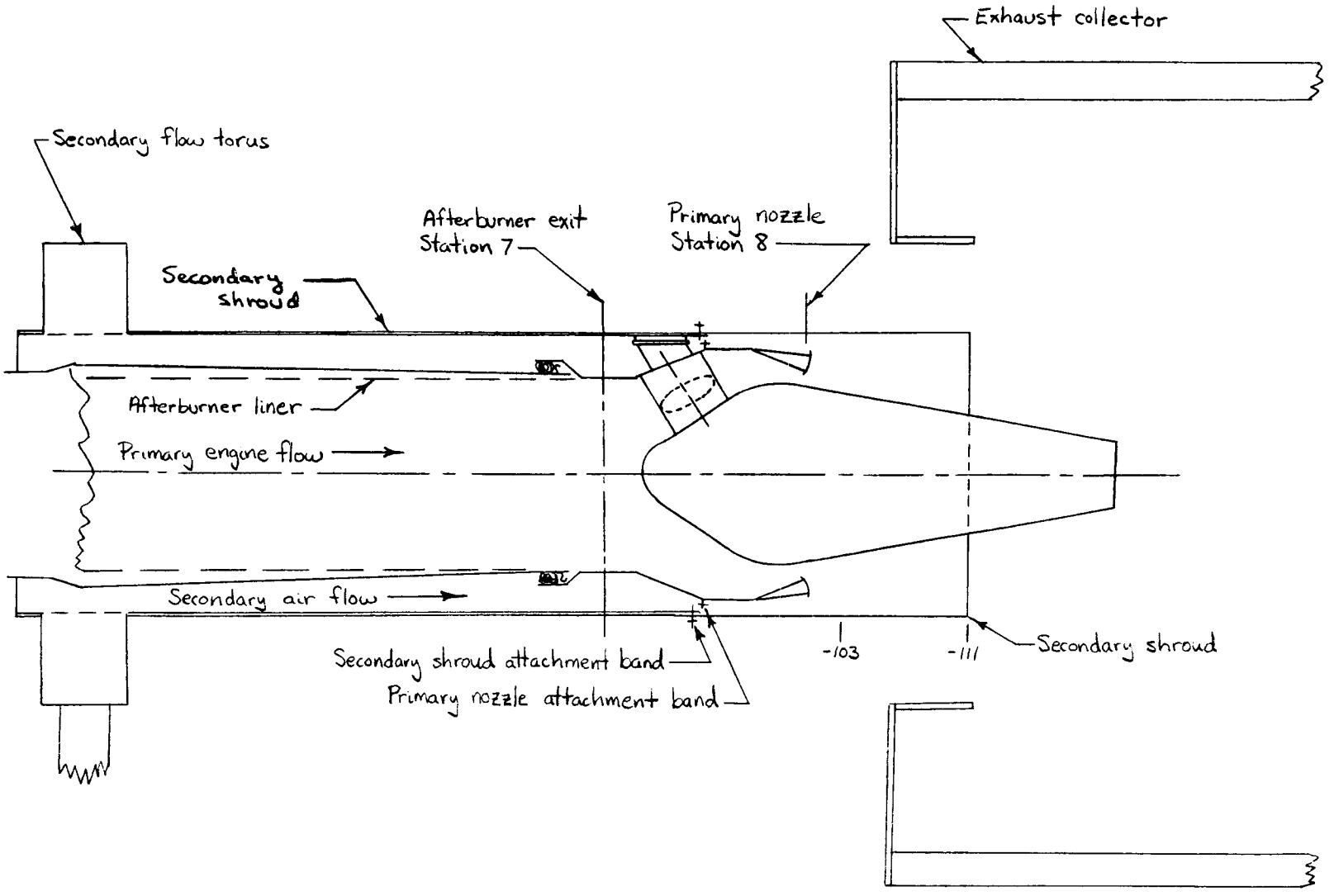

Figure 1.- Schematic diagram of nozzle test configuration

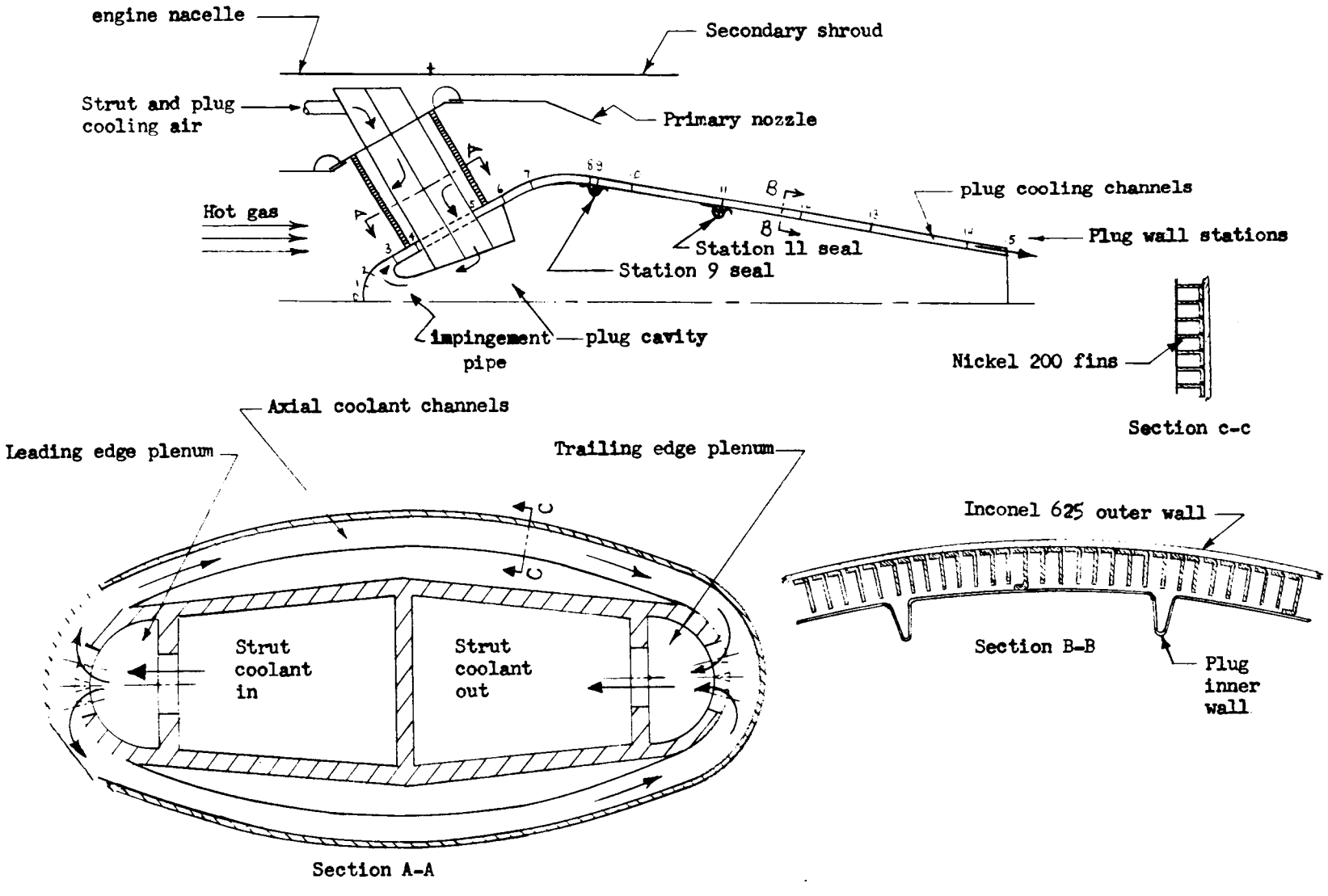

Figure 2 .- Strut and plug internal convection cooling configuration

E-5953

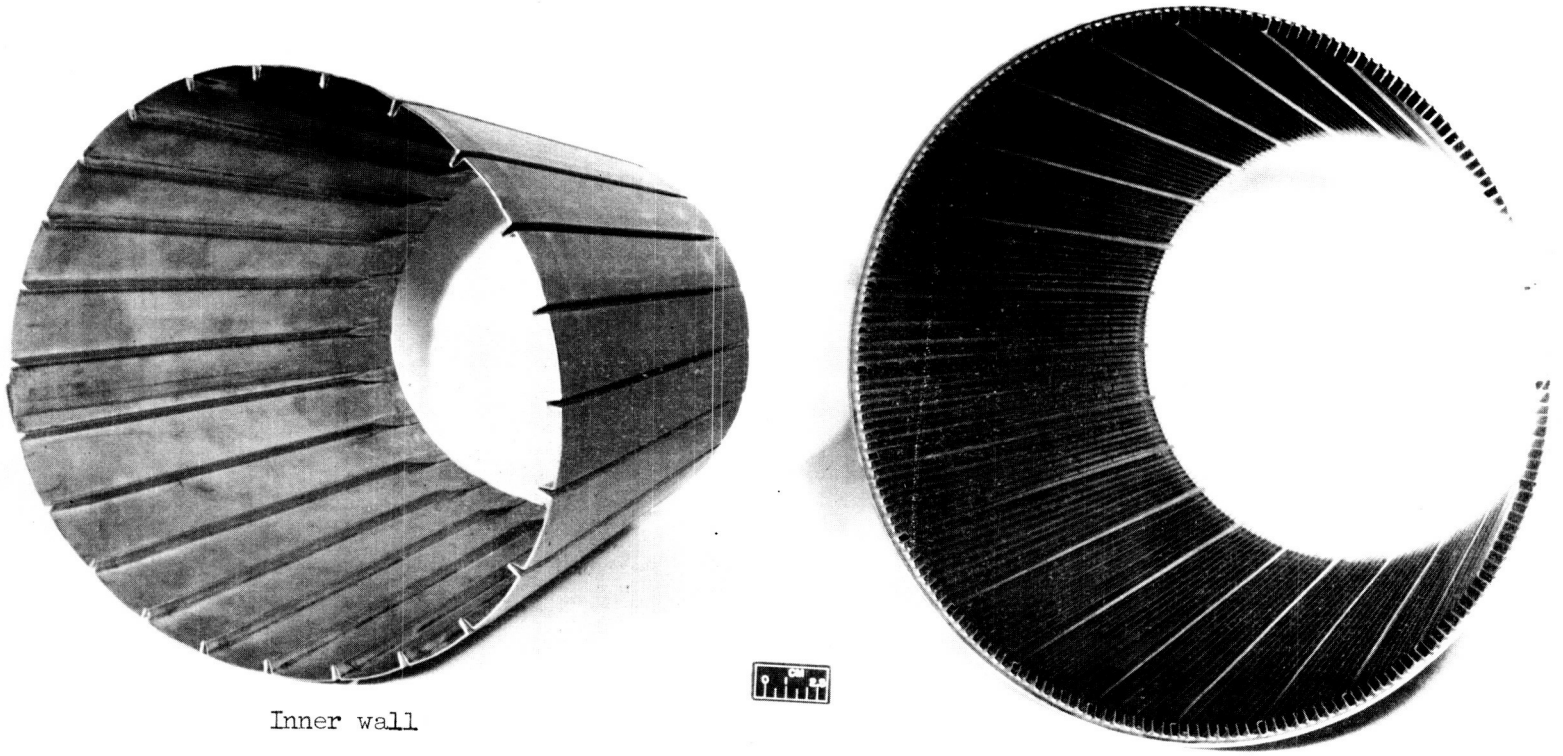

Inner wall

Outer wall with attached fins

C-68-2360

Figure 3 .- Plug nozzle segment showing inner wall on left and outer wall with attached fins on right

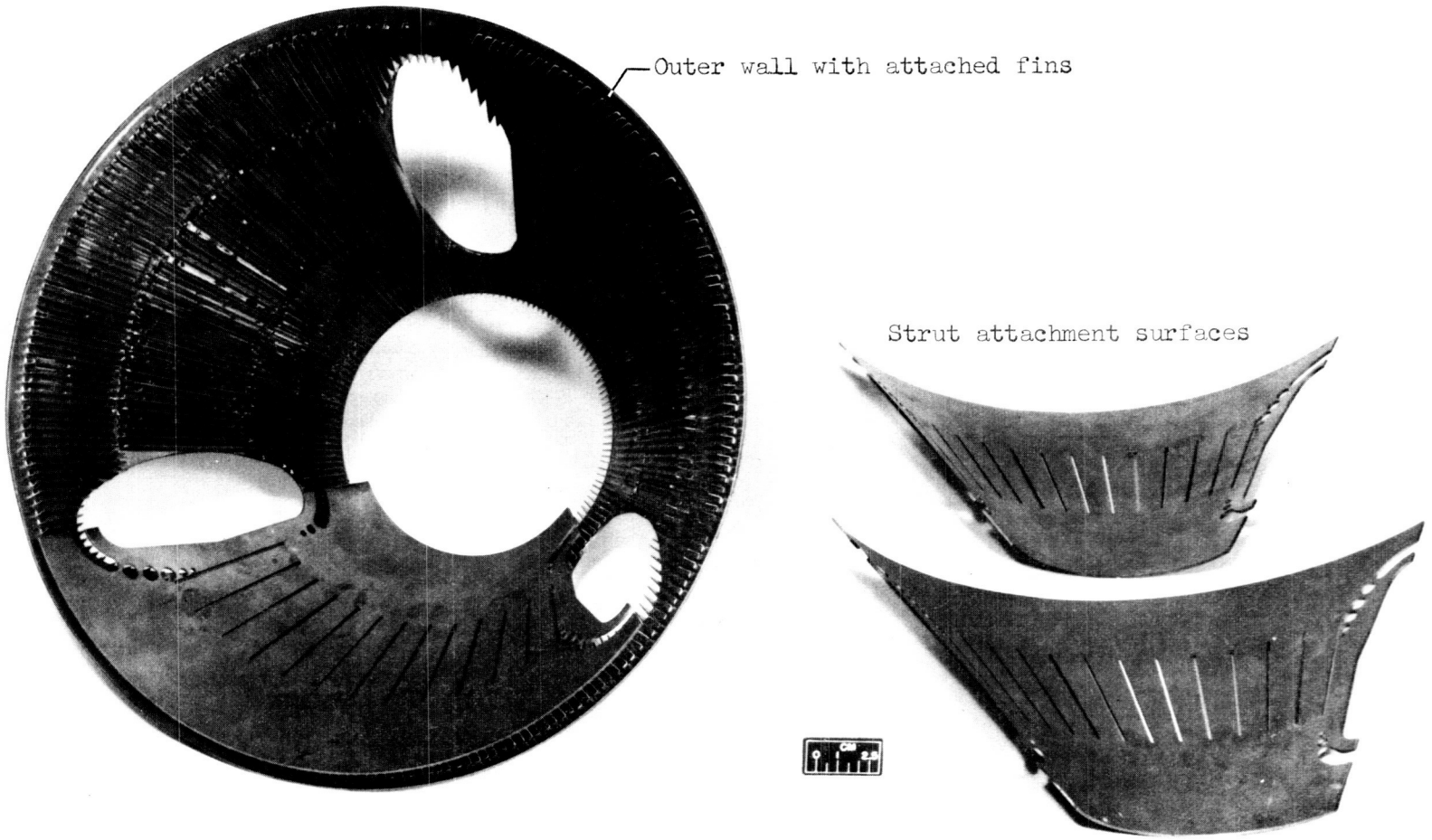

Figure 4 .- Plug nozzle segment showing strut attachment surfaces

E-5953

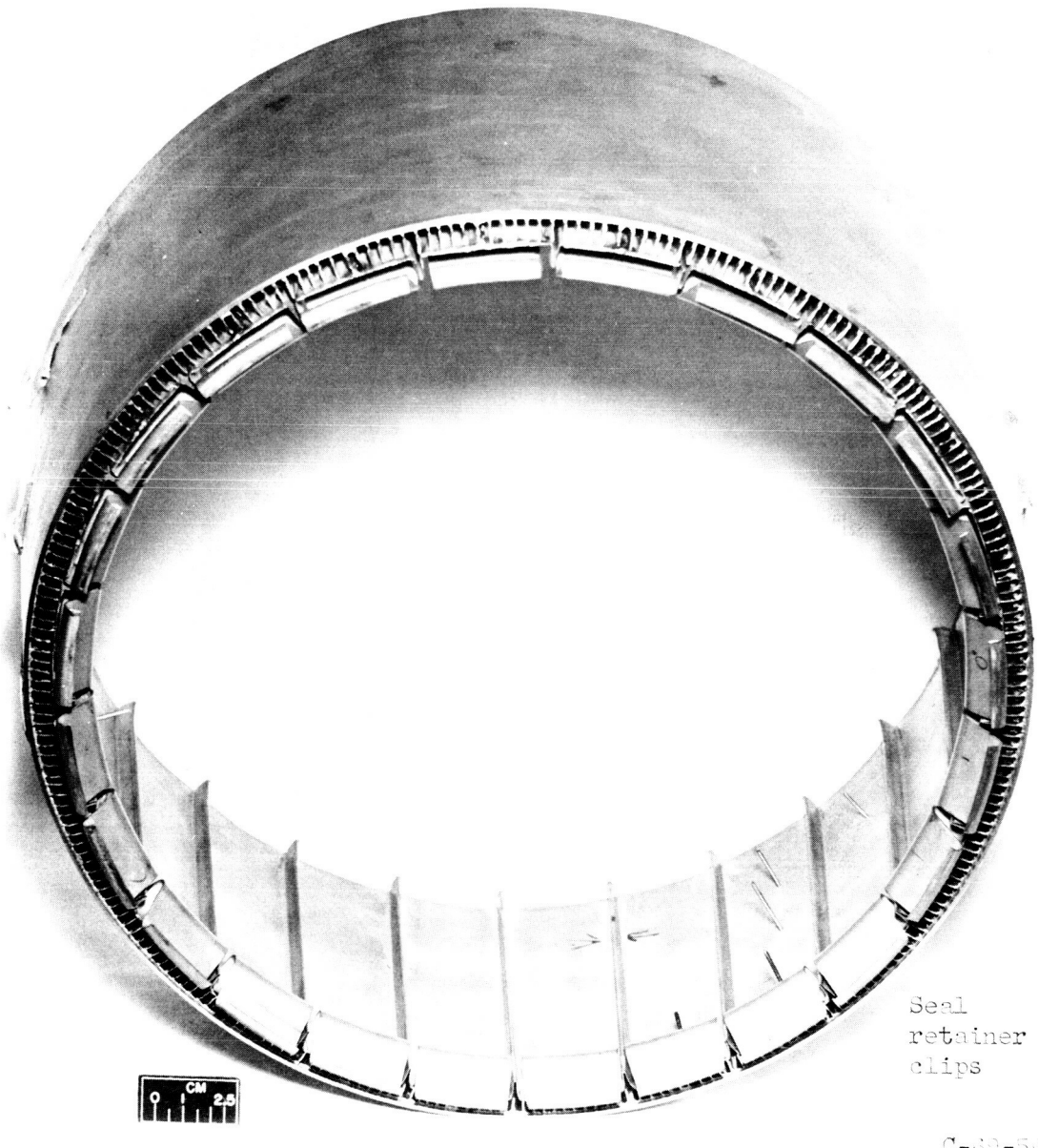

Figure 5 .- Assembled plug segment showing seal retainer clips

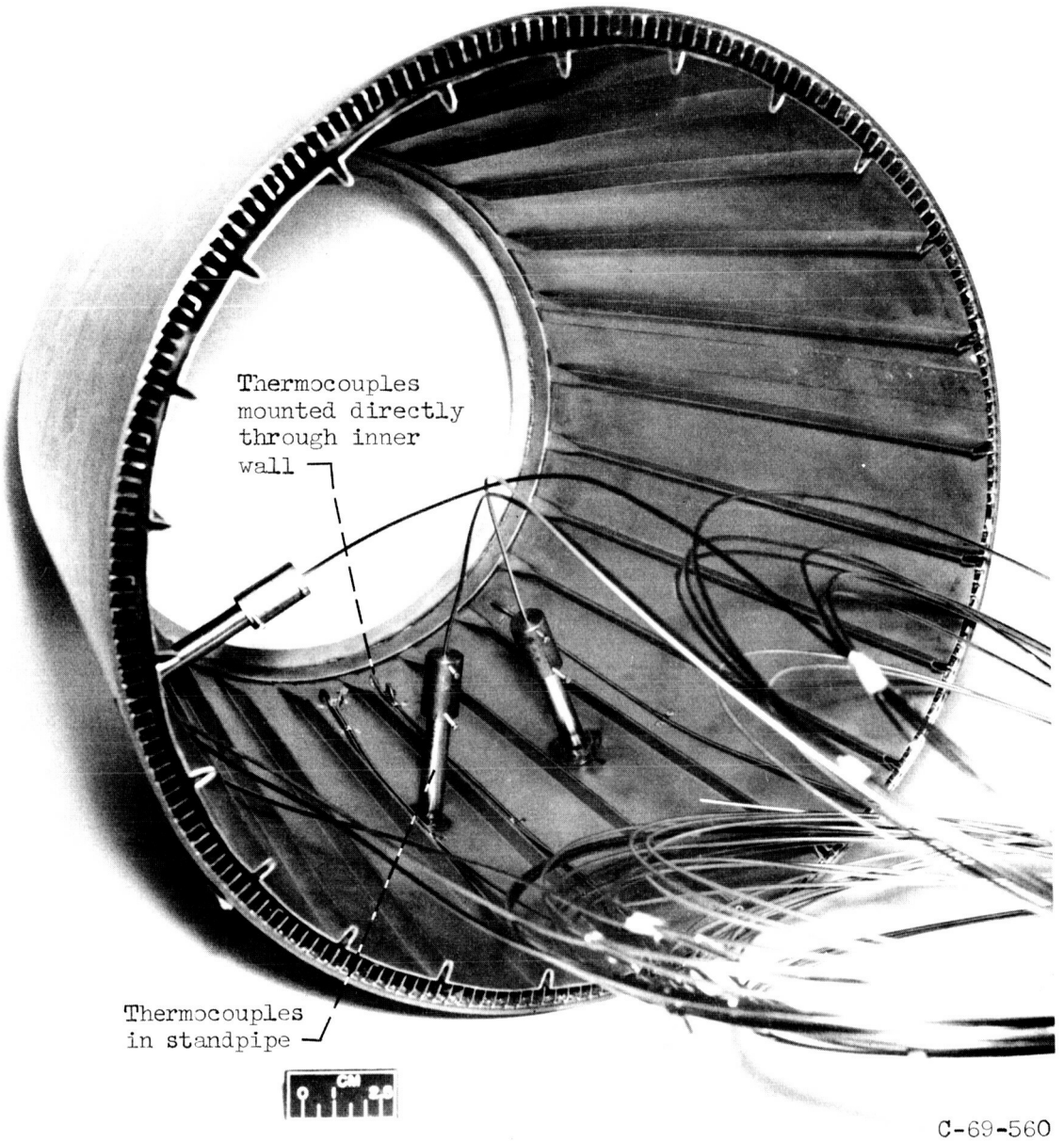

Figure 6 .- Assembled plug segment showing typical thermocouple installation

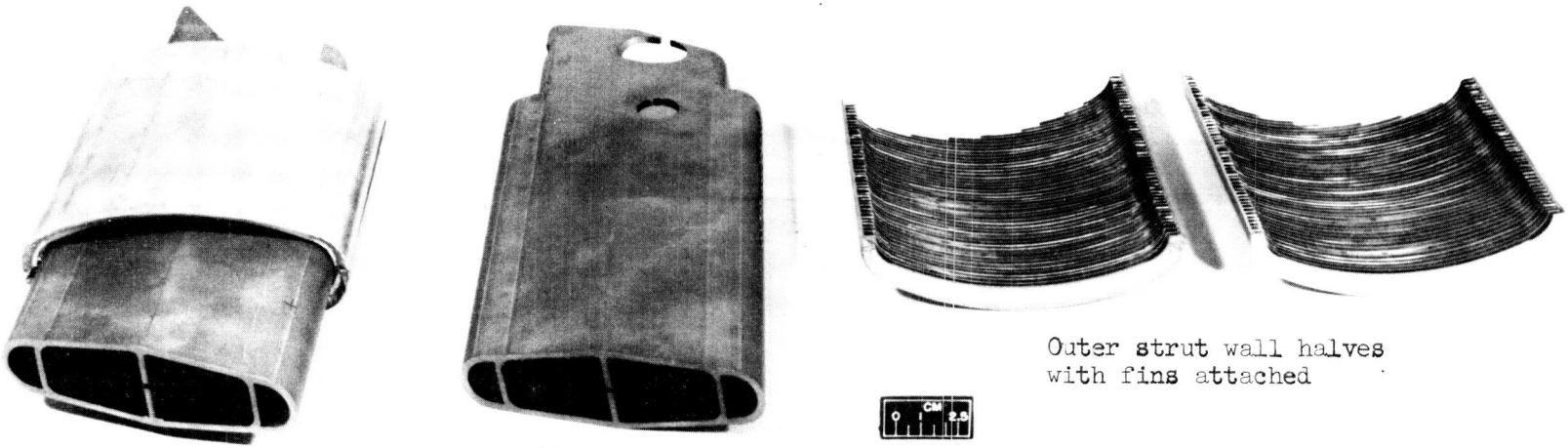

C-68-2364

Figure 7 .- Strut assembly

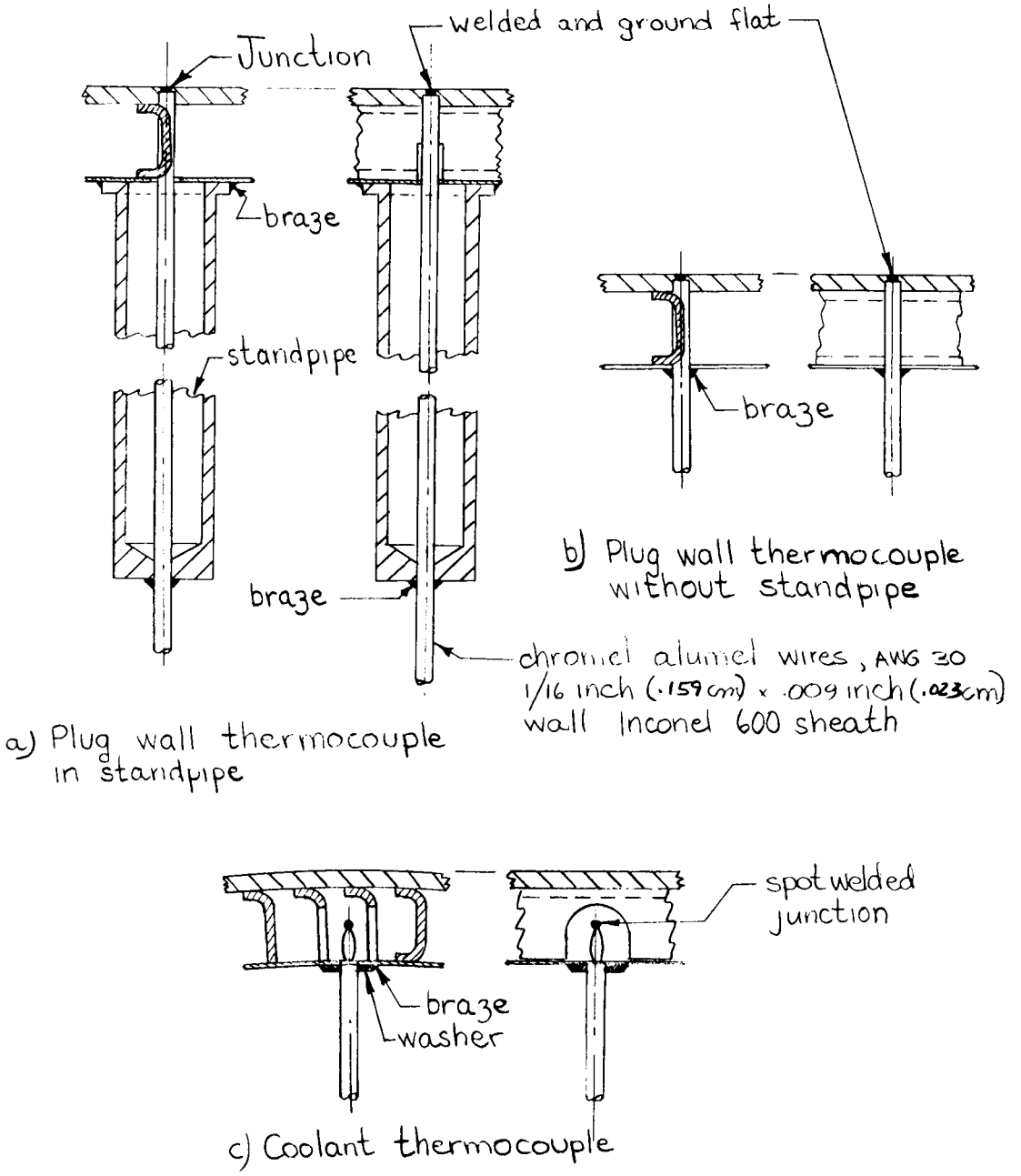

Figure 8 .- Plug thermocouple details

E-5953

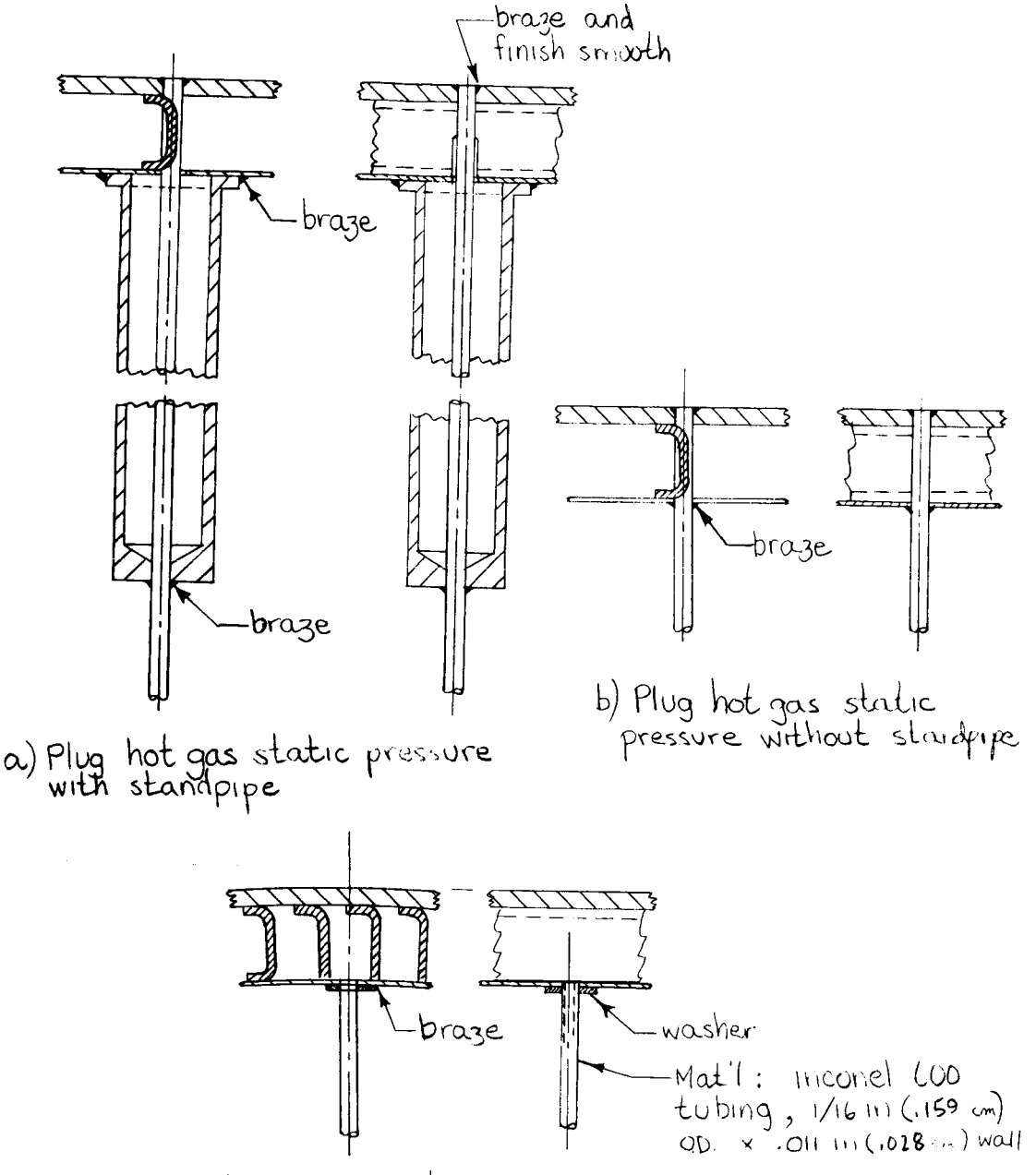

Figure 9 .- Typical plug static pressure taps

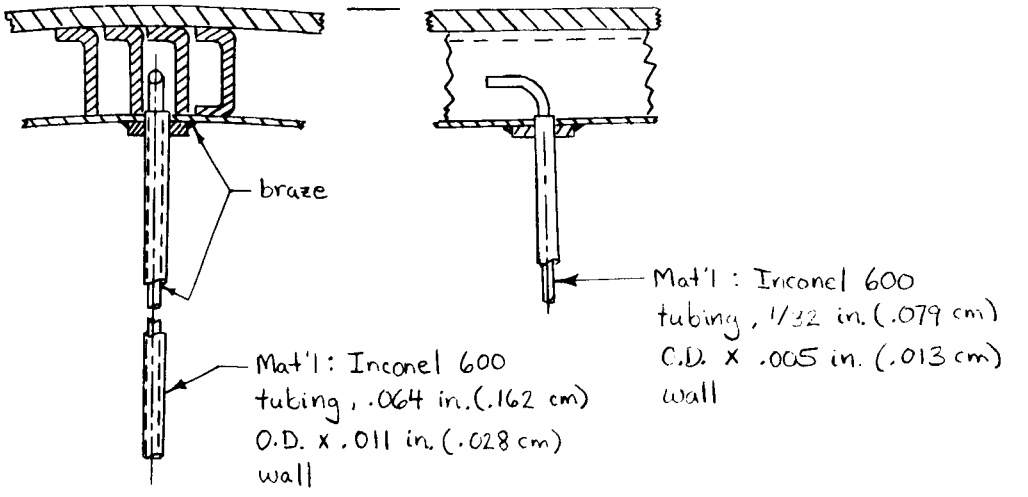

(a) Station - 8 coolant total pressure

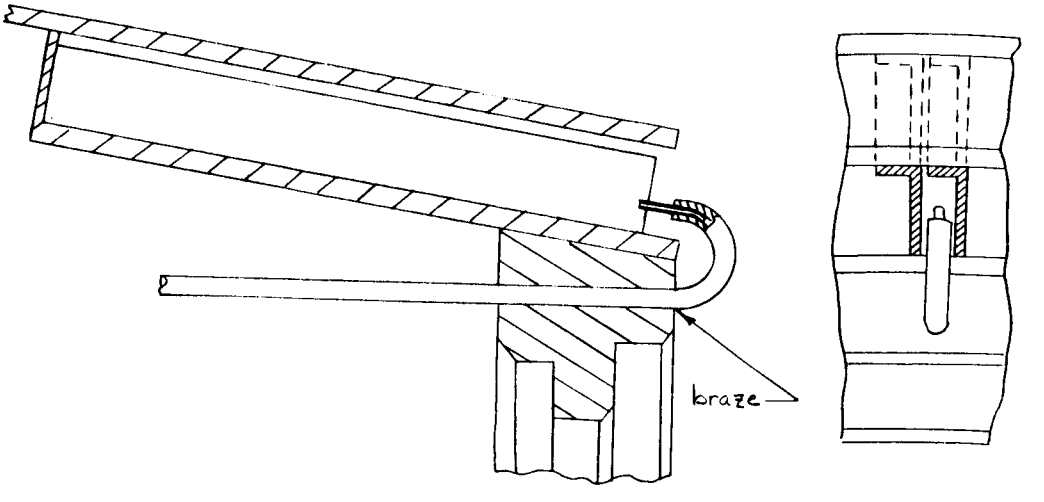

(b) Station - 15 coolant total pressure

Figure 10. - Coolant total pressure details

E-5953

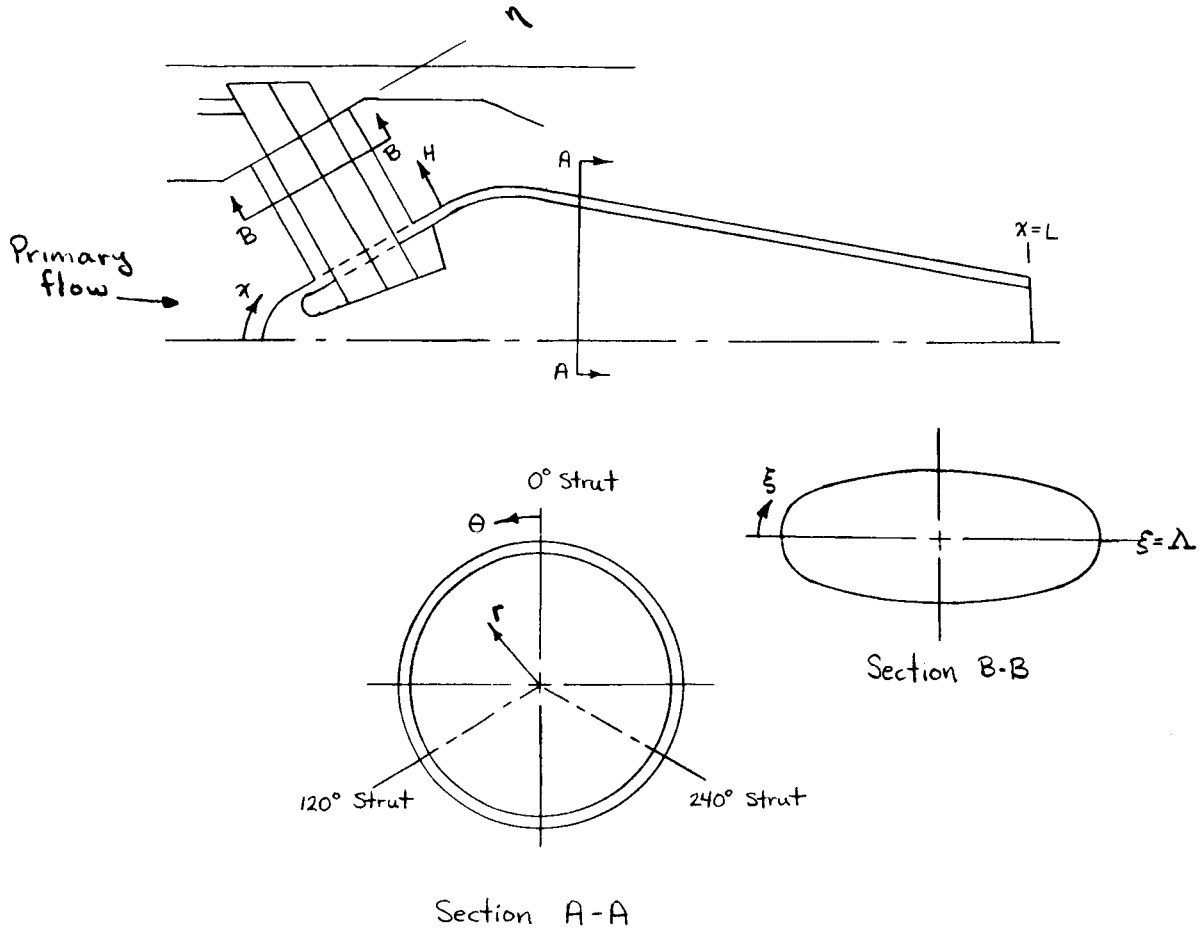

Figure 11. - Plug nozzle coordinate system used to locate instrumentation.

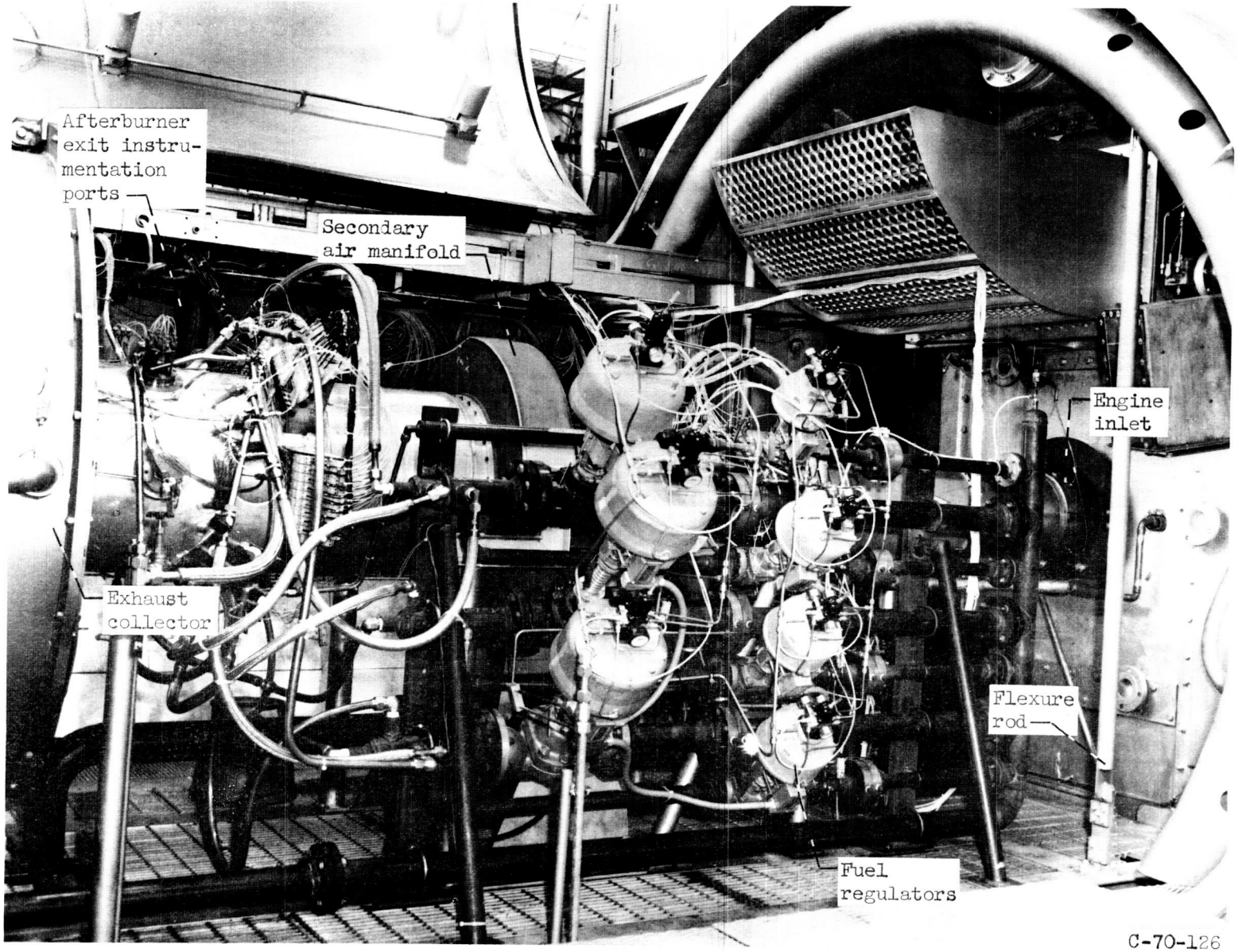

Figure 12.- Engine installation in Propulsion Systems Laboratory

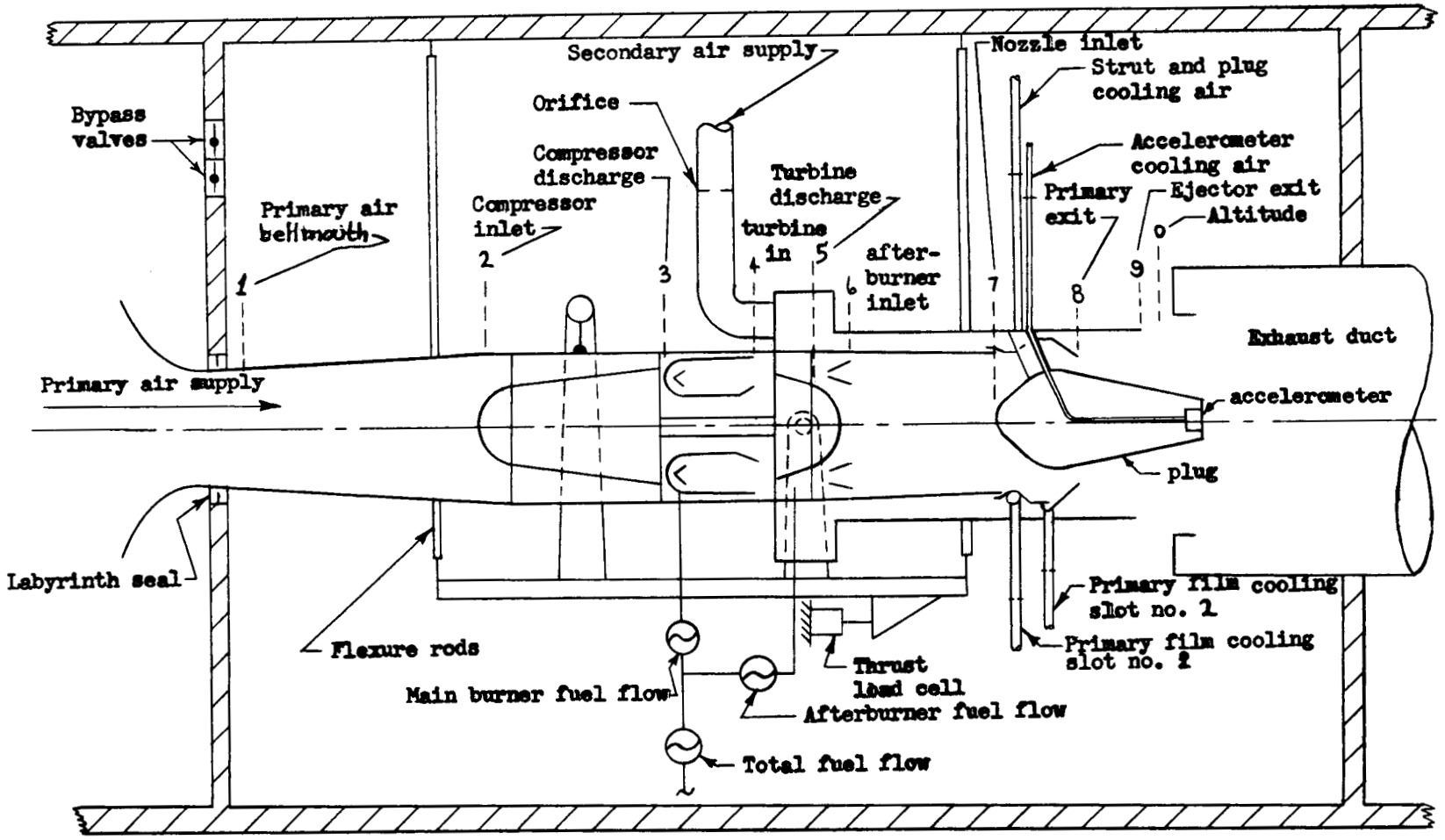

Figure 13.-Schematic of test installation

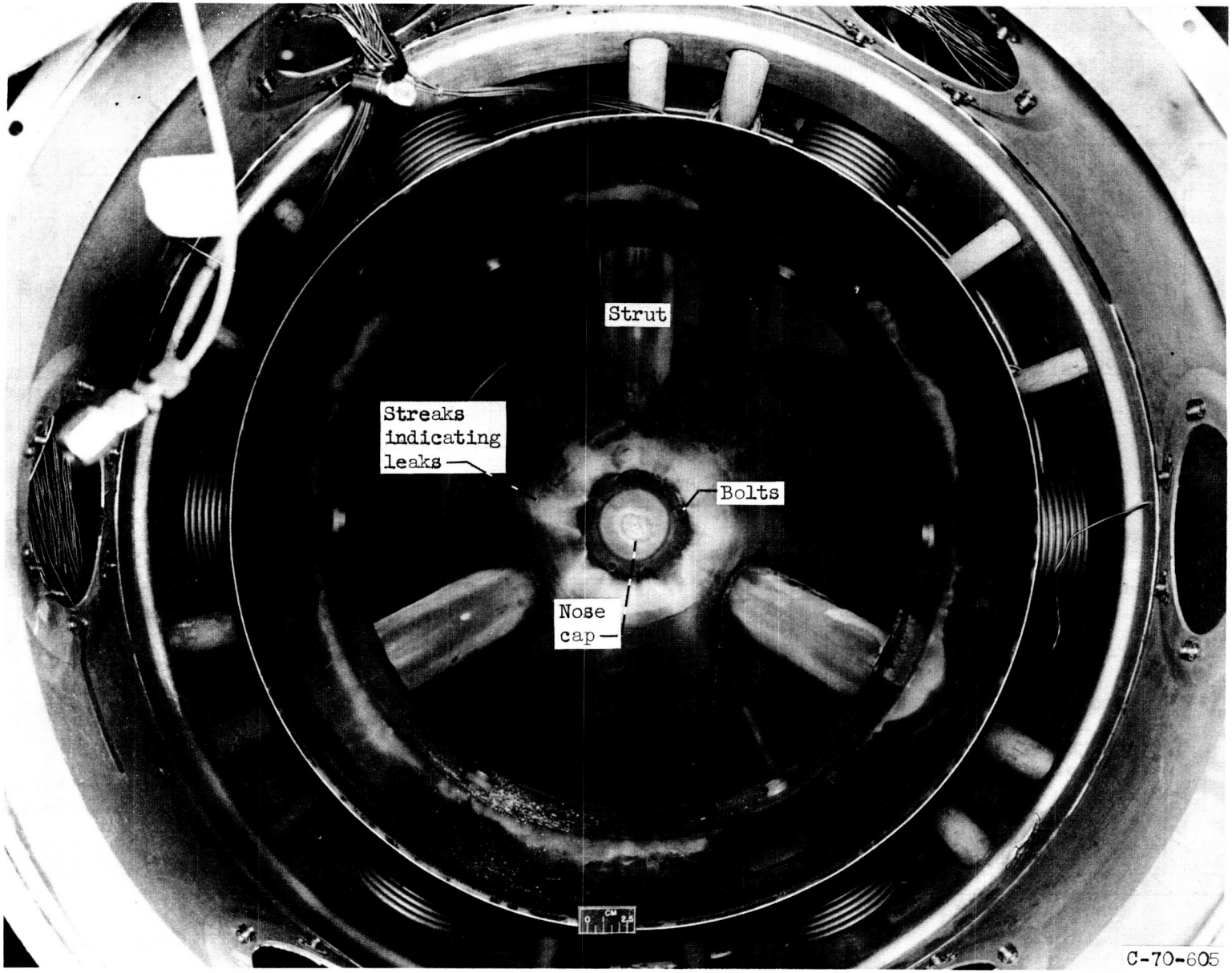

Figure 14.- Picture of plug leading edge showing cap leakage streaks

E-5953

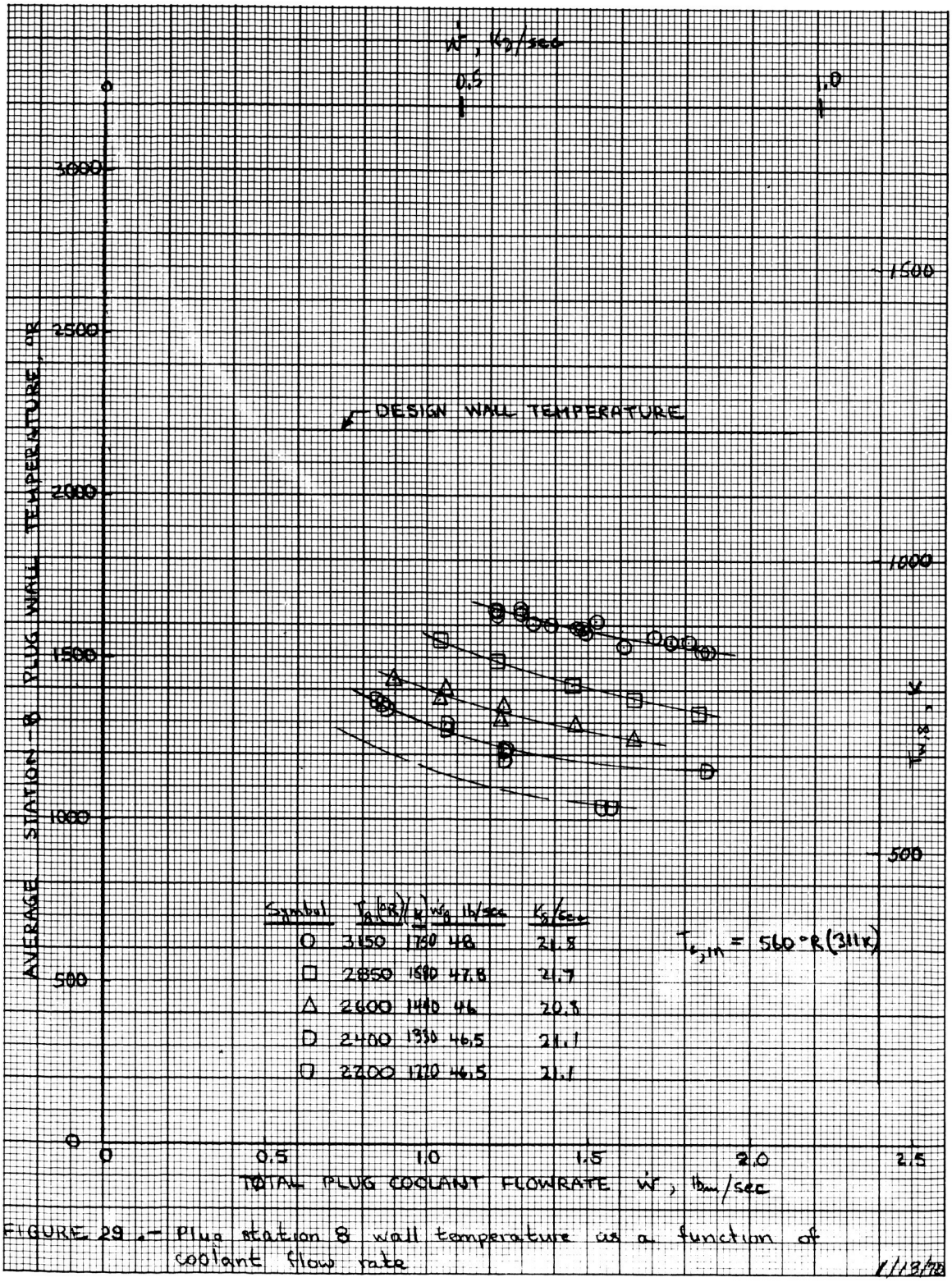

Symbol	$T_{c,in}$ (°R)/(K)	$\dot{W}_c$ lb/sec	K_s/c_{cr}
○	560 / 311	48	21.8
□	560 / 311	47.8	21.7
△	560 / 311	46	20.8
▽	560 / 311	46.5	21.1
◇	560 / 311	46.5	21.1

FIGURE 29.- Plug station 8 wall temperature as a function of coolant flow rate

1/13/72

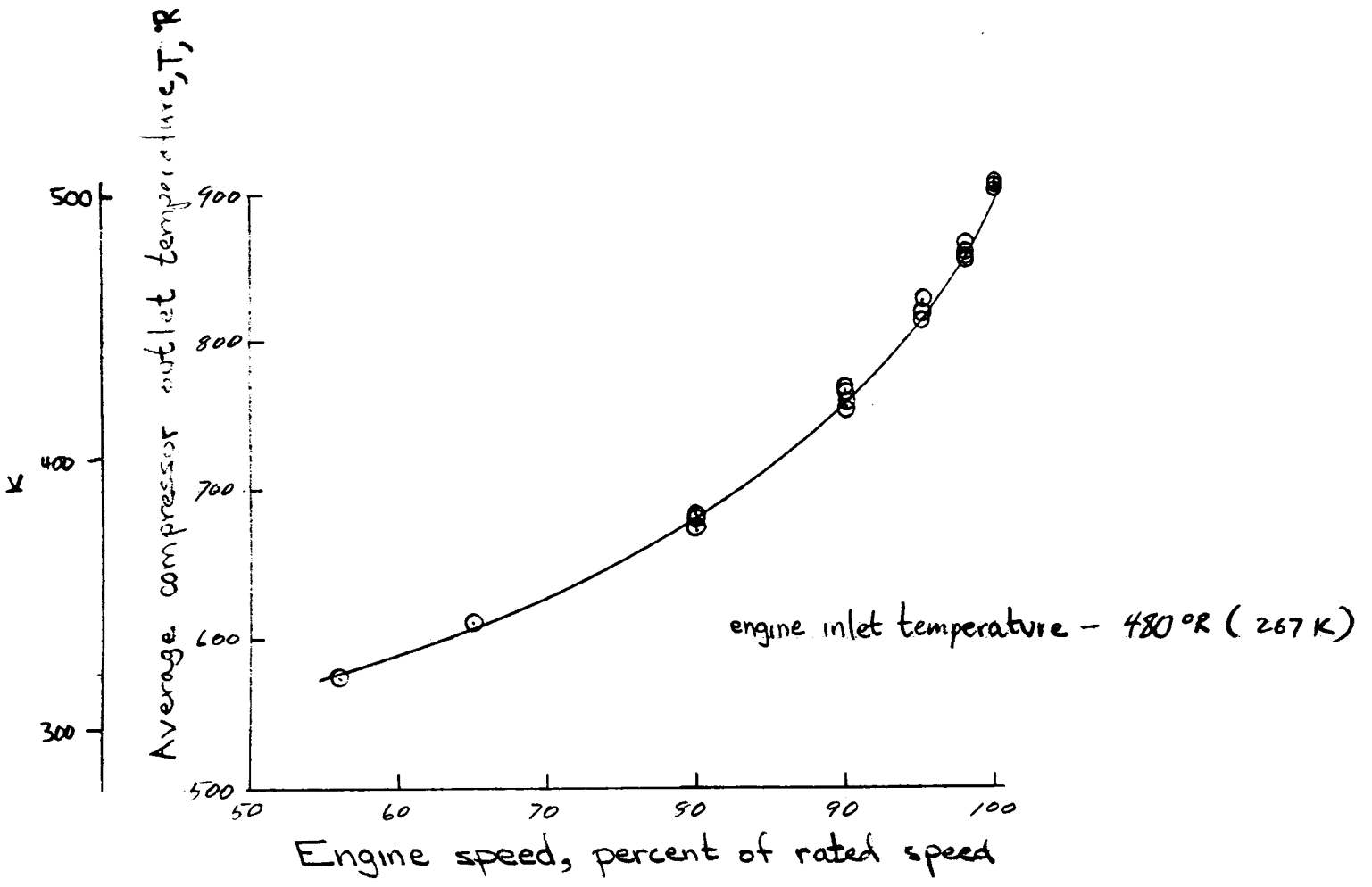

Figure 16 .- Compressor outlet temperature as a function of engine speed

E-5953

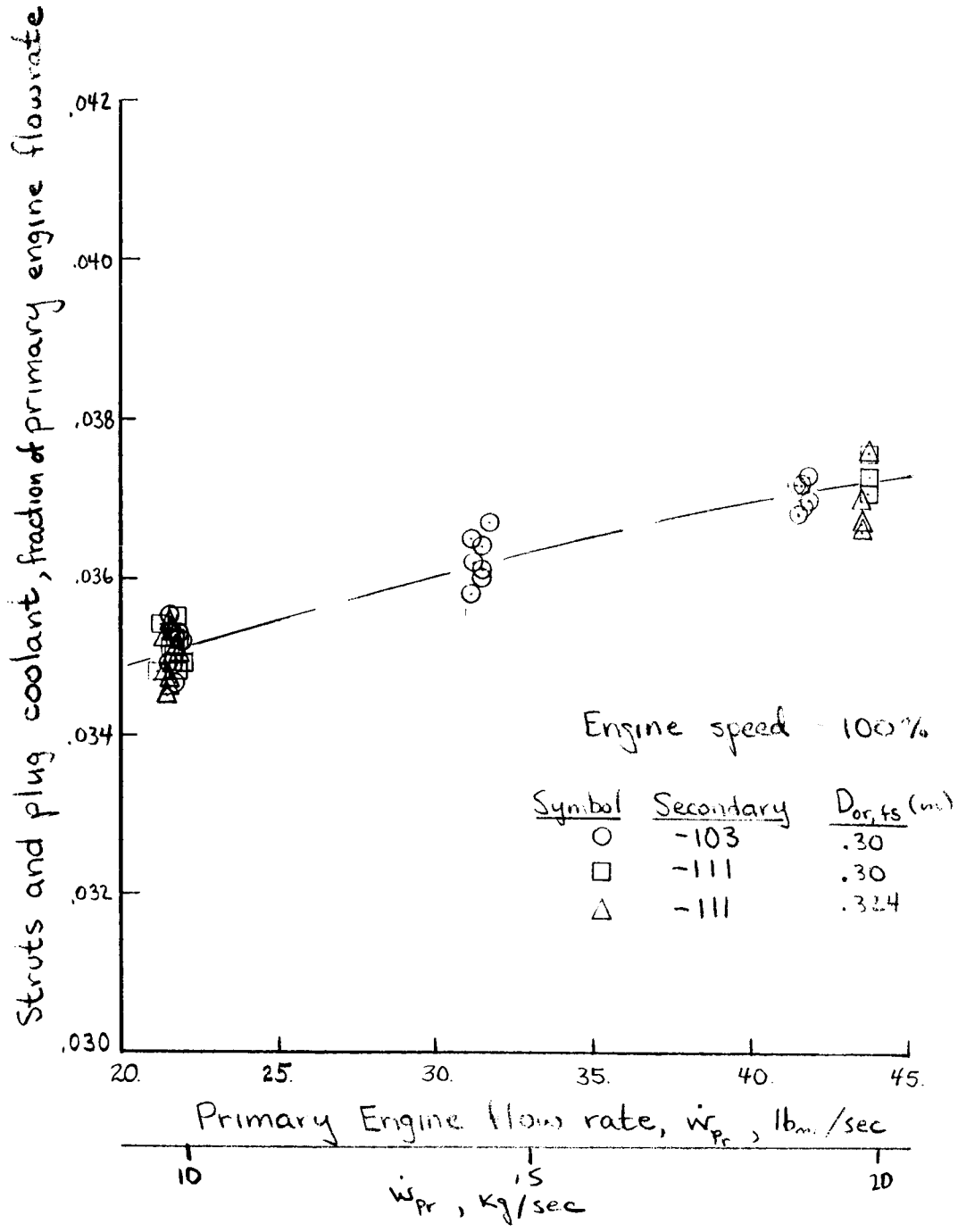

Figure 17 .- Coolant flowrate to struts and plug for compressor discharge runs.

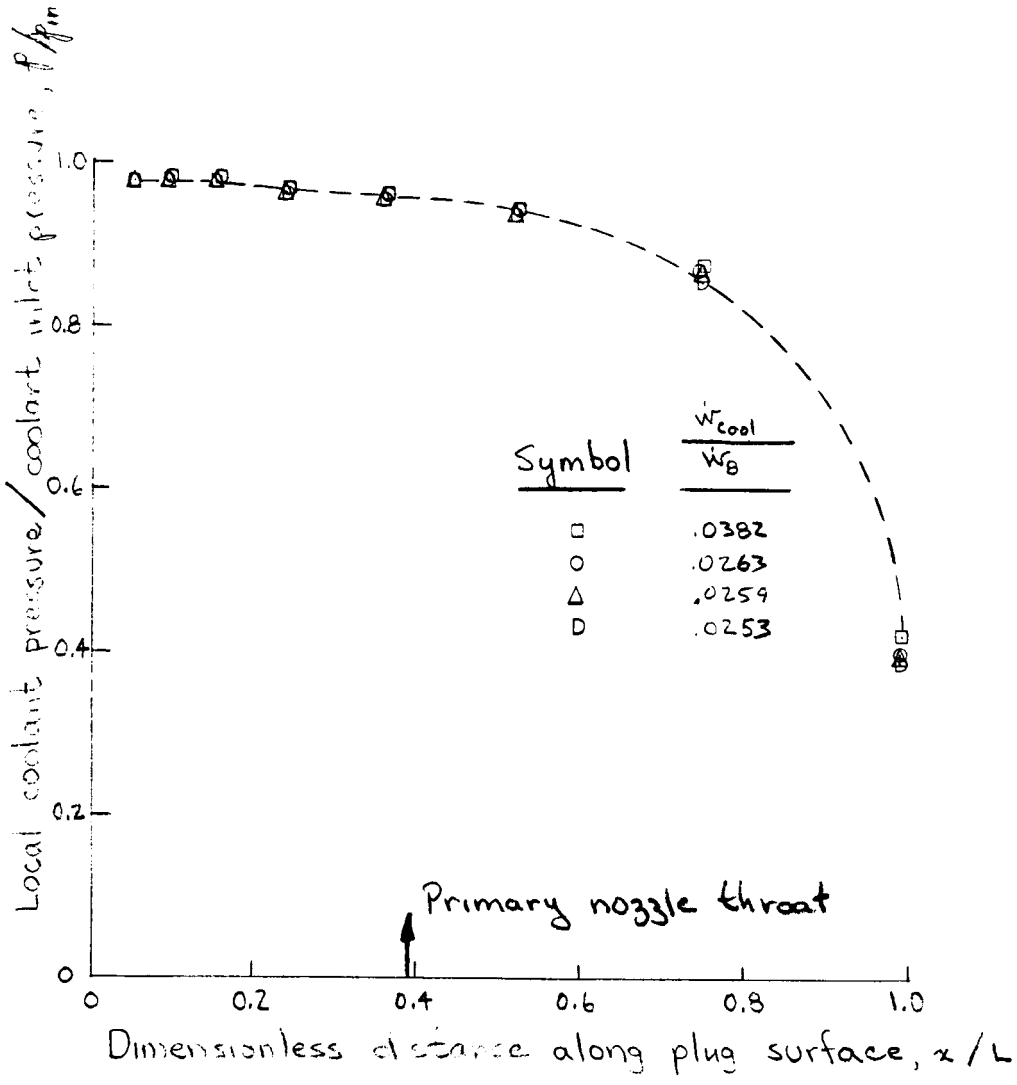

Figure 18.- Plug coolant pressure distribution

E-5953

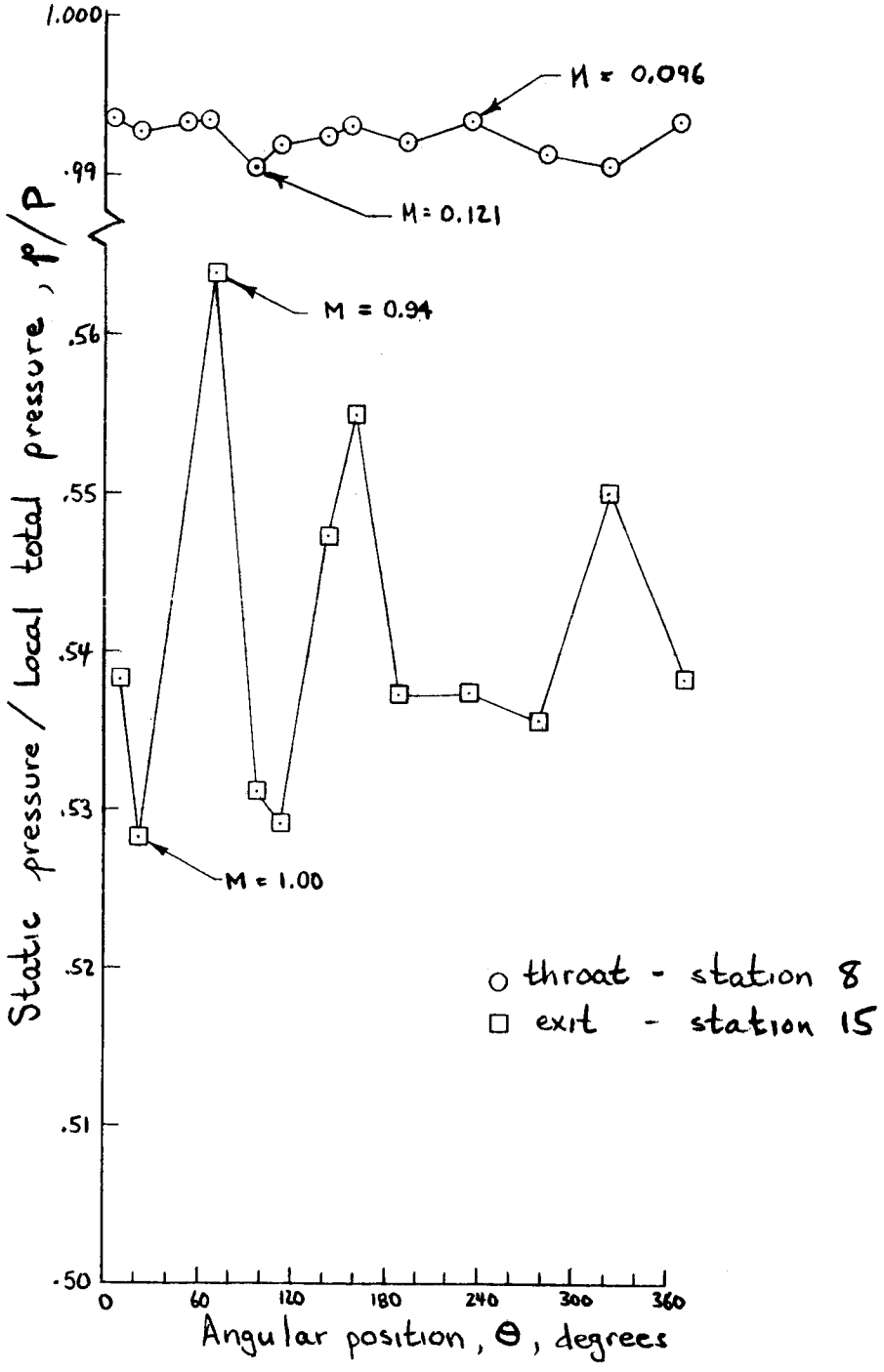

Figure 19.- Coolant circumfirential static/total pressure ratios

Symbol	P_8/P_a	P_8 (atm)	$\dot{W}_8$ (lbm/sec)	$\dot{W}_8$ Kg/sec
○	2.27	1.81	53.68	24.33
□	3.50	1.80	53.21	24.13
△	5.51	1.79	53.11	24.07
▽	6.39	1.77	52.42	23.78
▷	7.95	1.77	52.26	23.70
◇	11.86	1.77	52.56	23.80

Primary nozzle area, 130 in² (838 cm²)
Non-afterburning, T_8 = 1260°R (700 K)

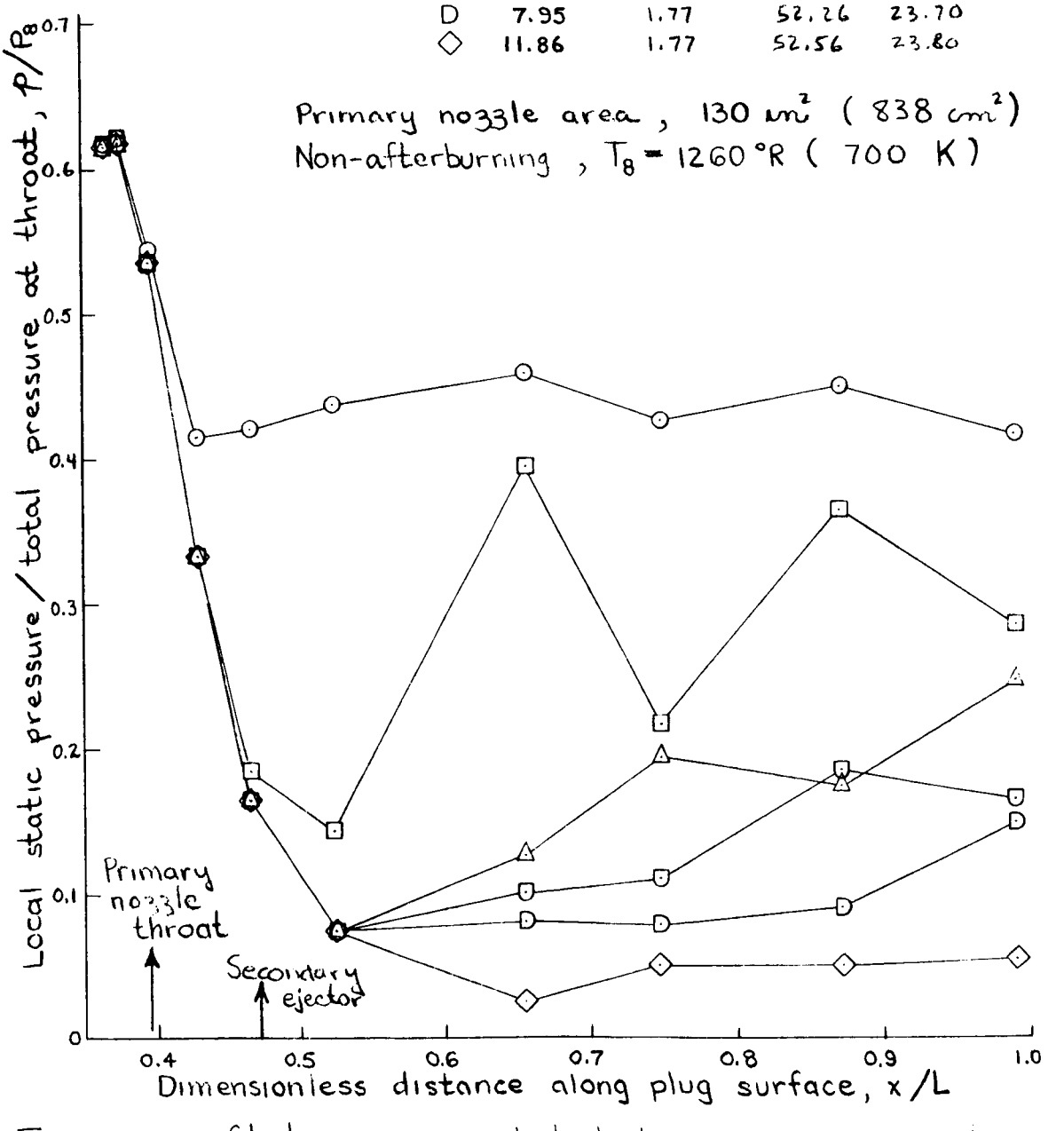

Figure 20.- Static pressure distributions in supersonic stream - effect of pressure ratio

6/23/70

E-5953

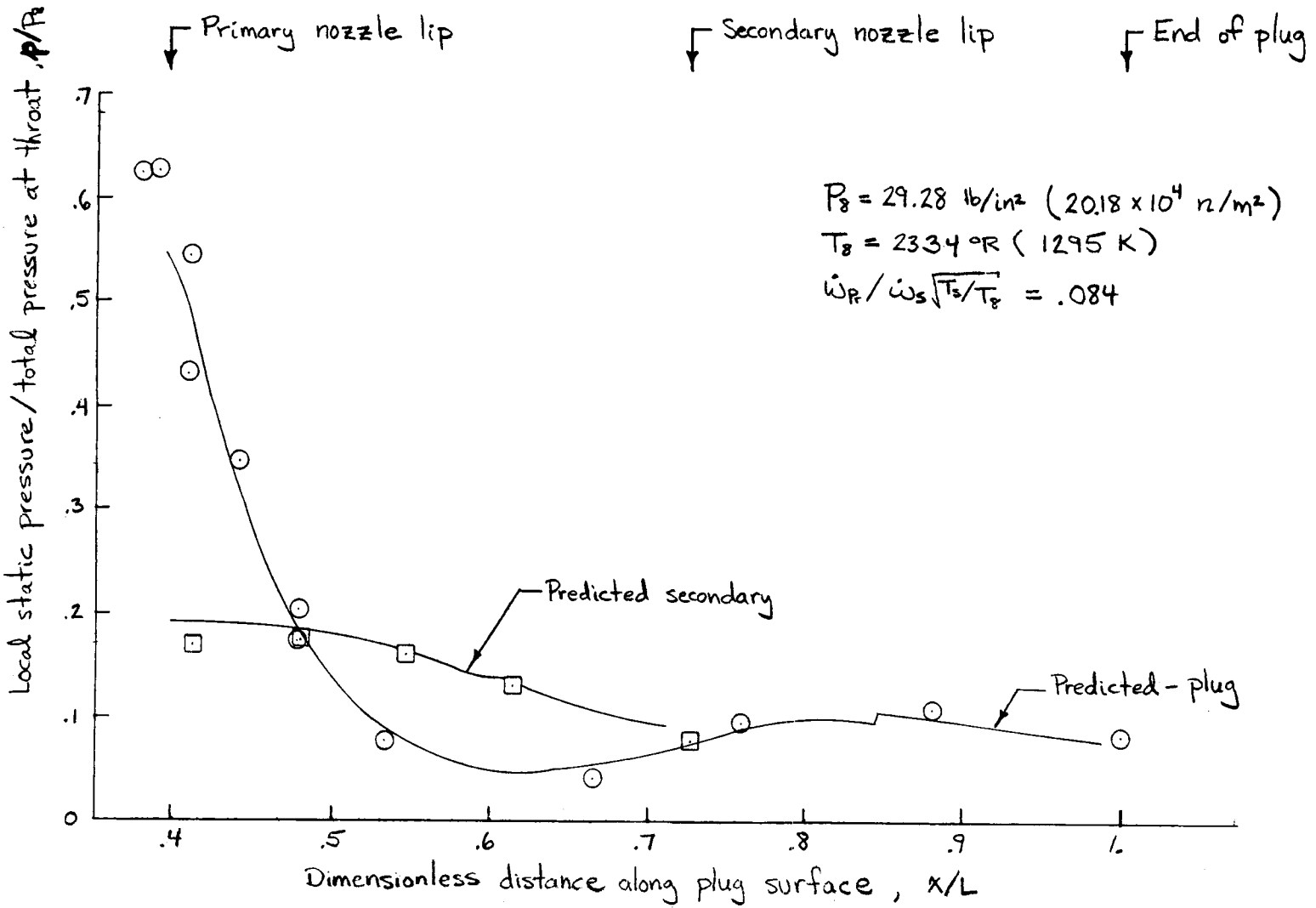

Figure 21. - Comparison of measured and predicted local static pressure

Symbol	P_B/P_o	P_B (atm)	$\dot{W}_B$ (lbm/sec)	(kg/sec)	x/L Secondary	T_B (°R)
□	3.32	1.78	41.78	18.95	.471	3025
◺	3.24	.923	22.04	10.00	.72	3020

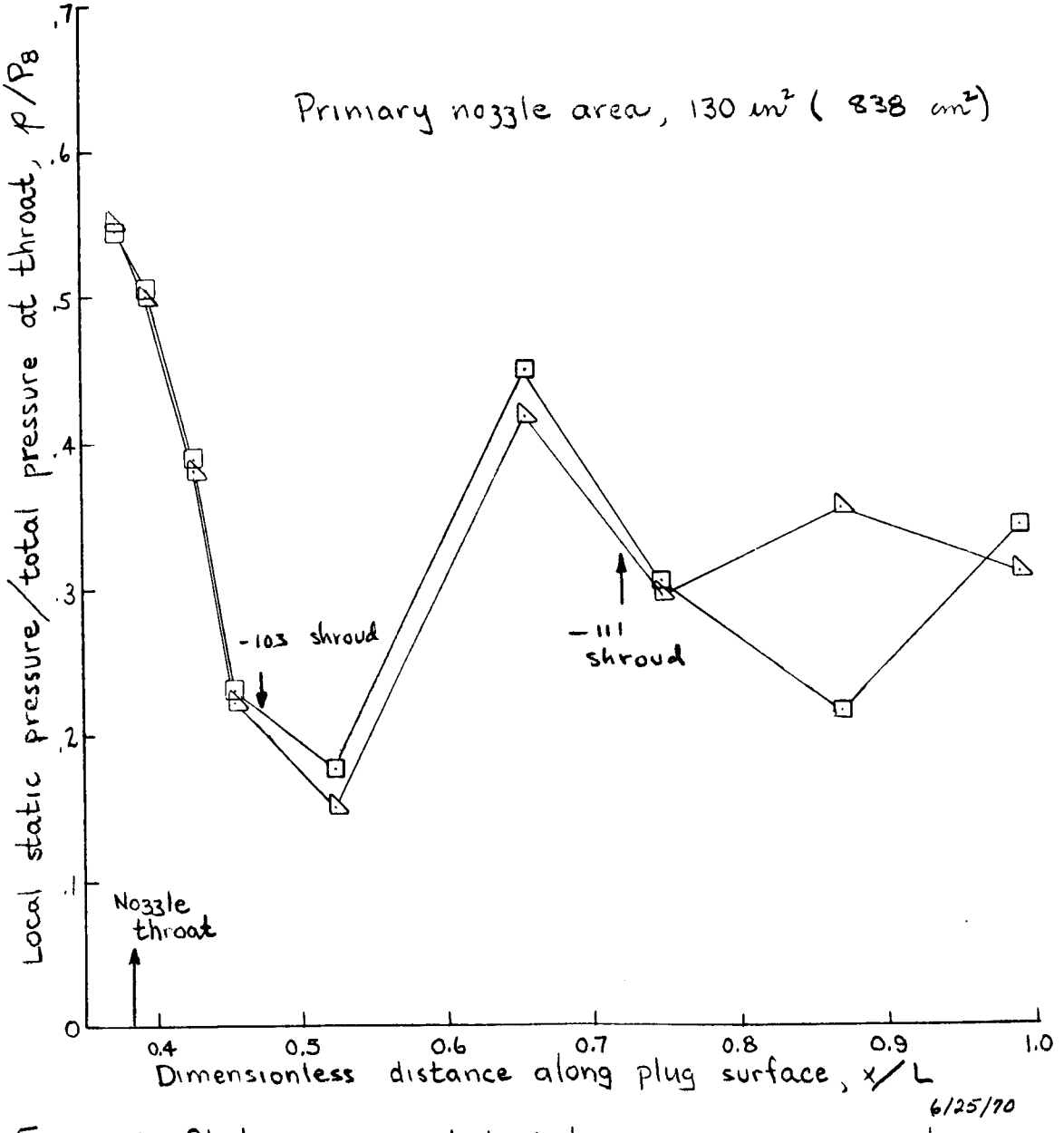

6/25/70

Figure 22.- Static pressure distributions in supersonic stream - effect of shroud length

E-5953

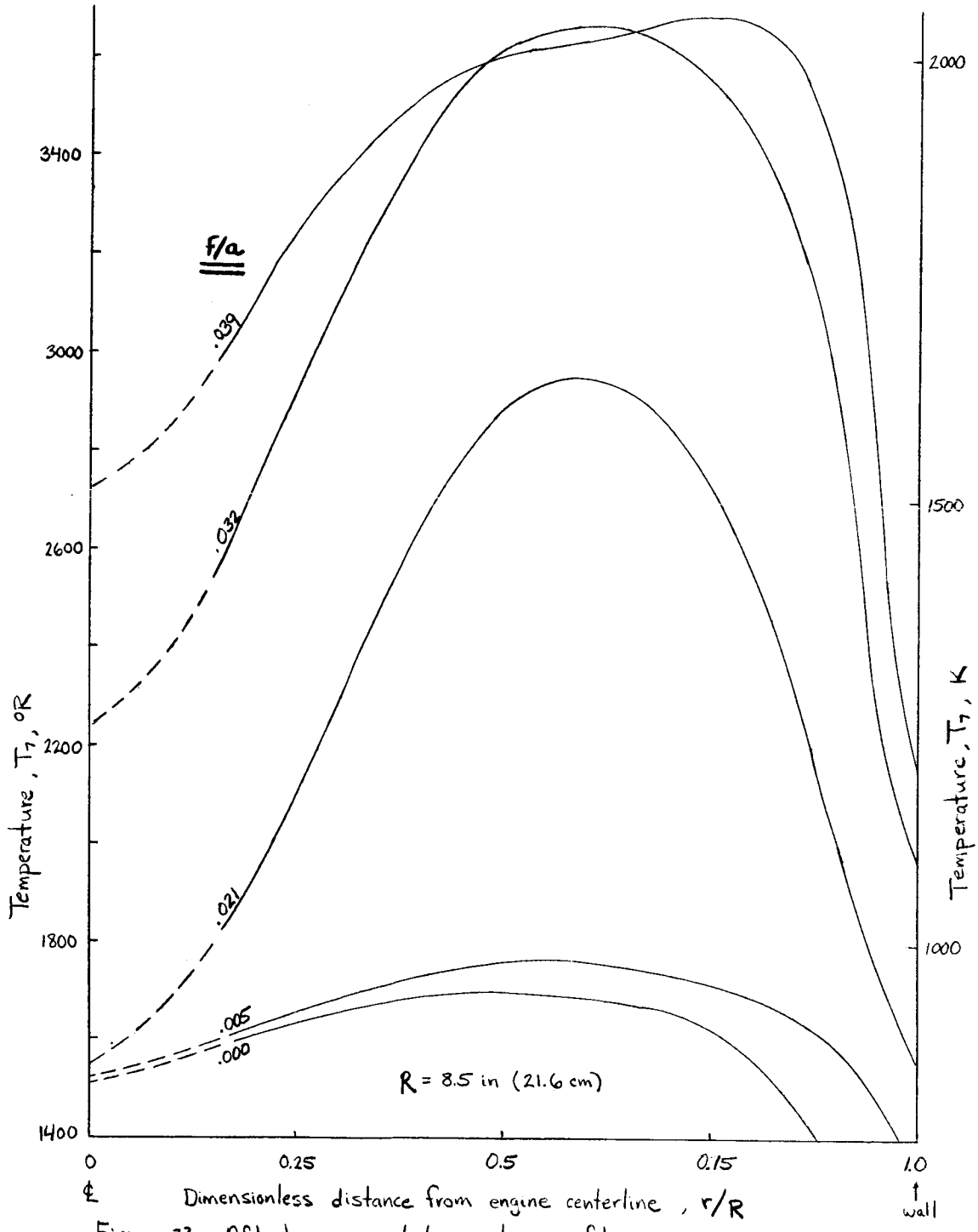

Figure 23.- Afterburner exit temperature profiles

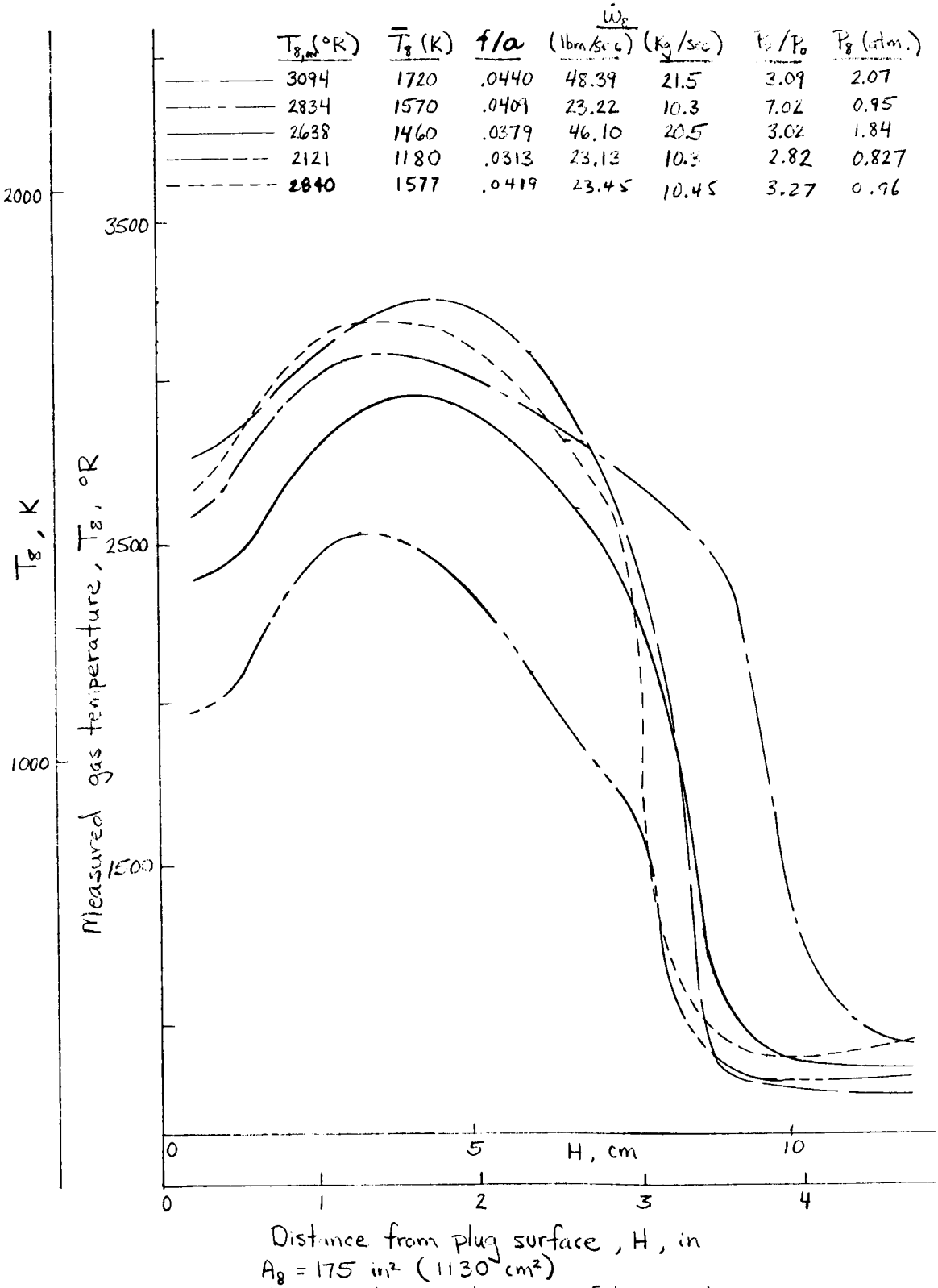

Figure 24. - Hot gas temperature profiles - station 8

E-5953

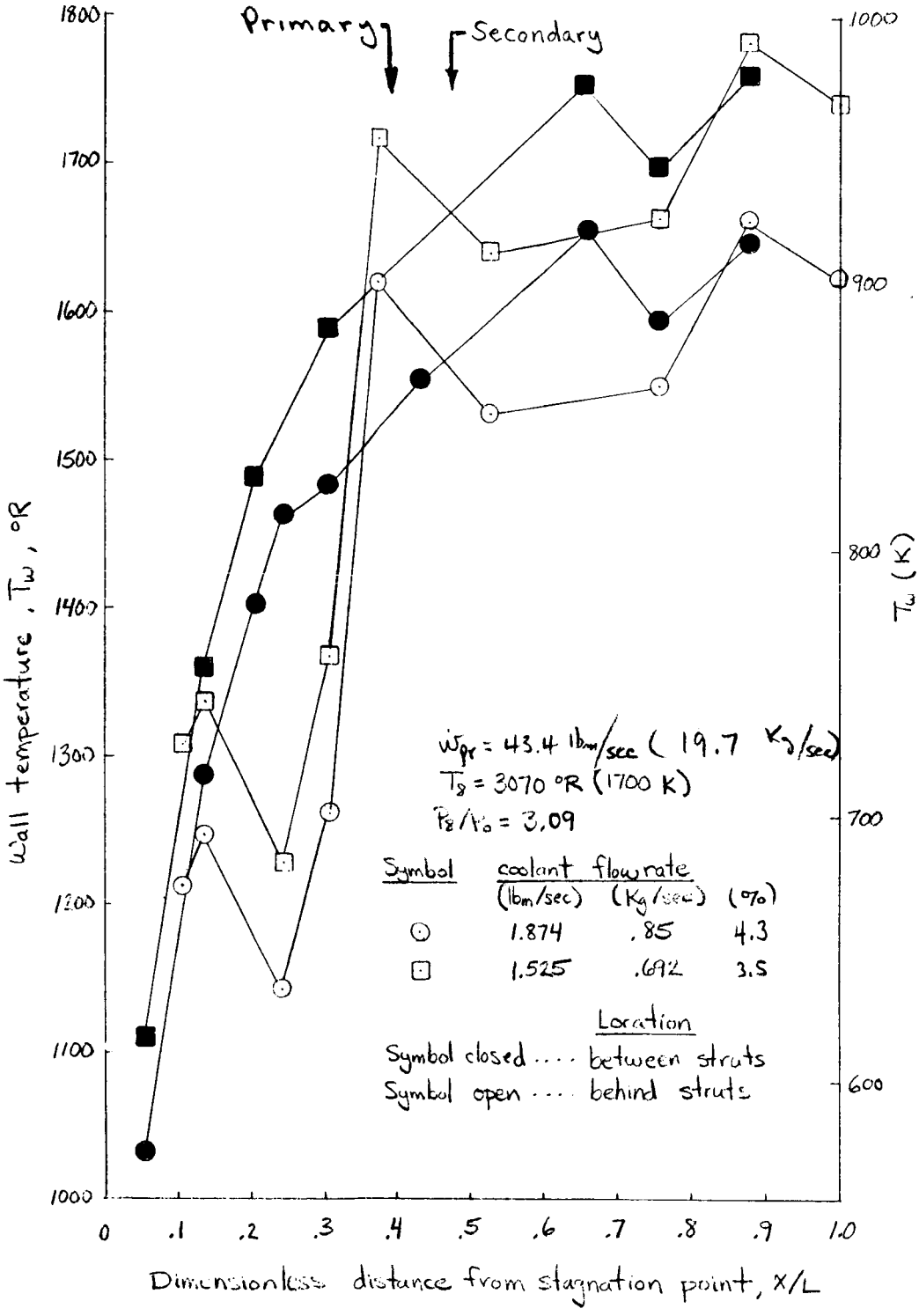

Figure 25. - Effect of coolant flowrate on plug wall temperatures

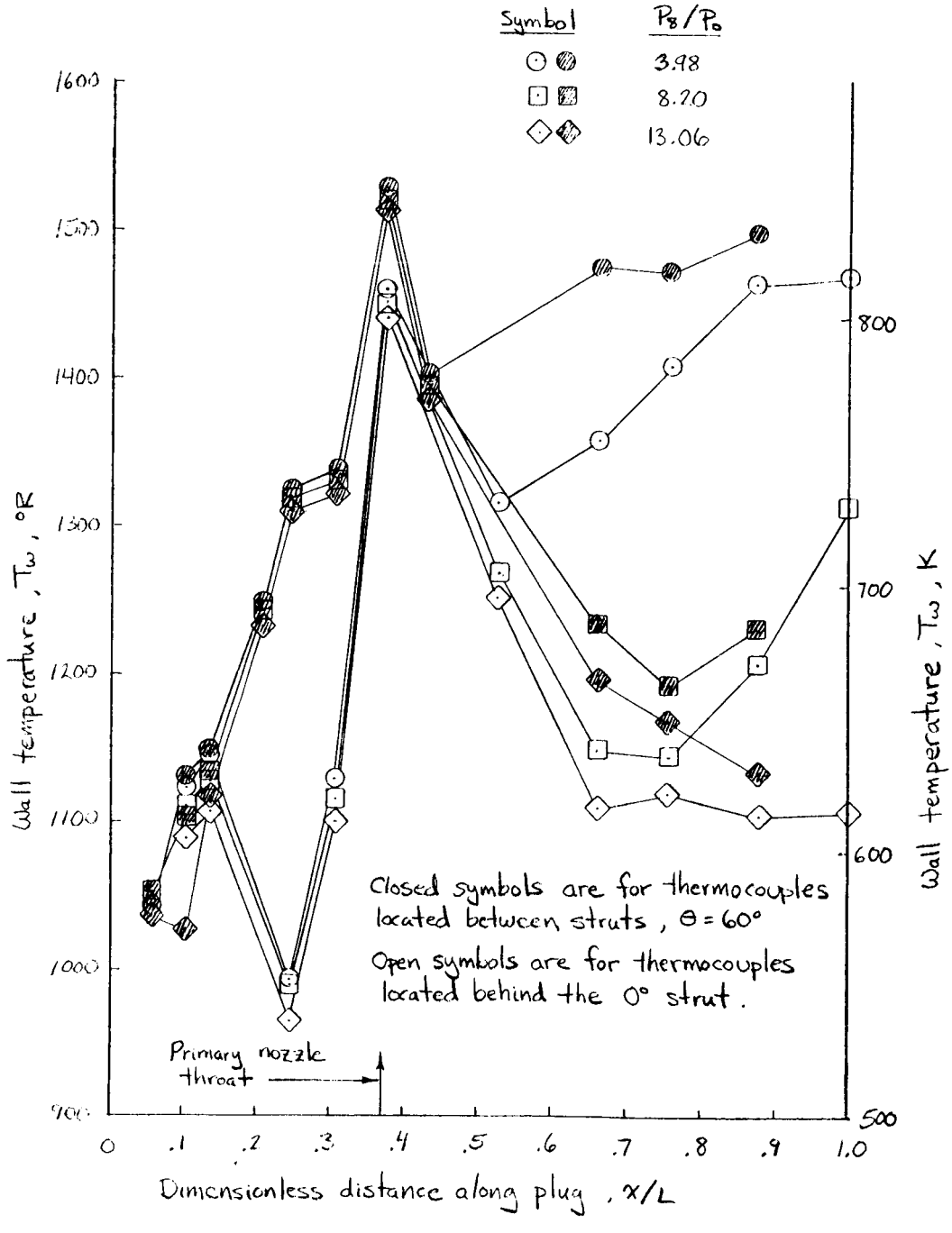

Figure 26. – Effect of nozzle pressure ratio on plug wall temperatures

E-5953

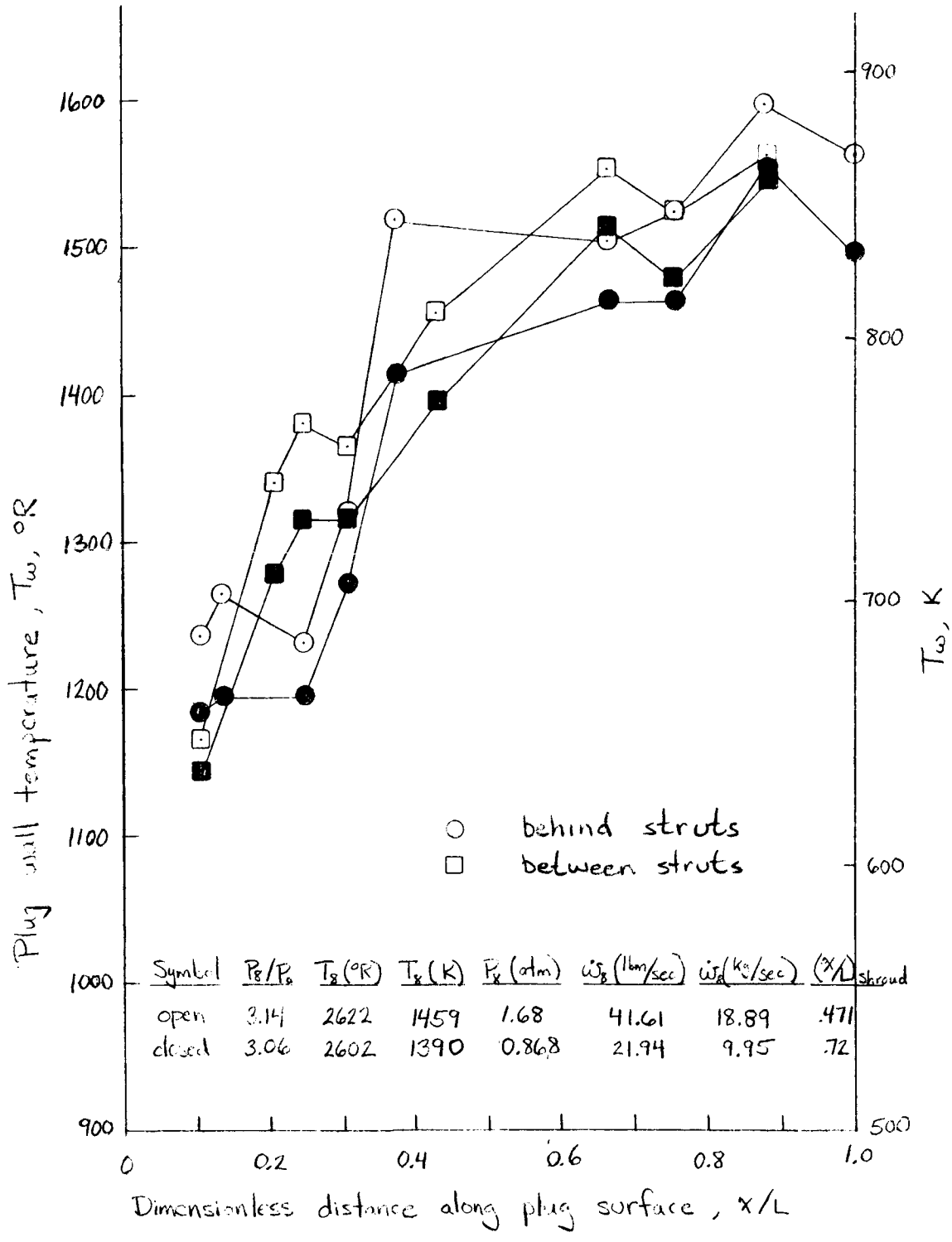

Figure 27. - Effect of engine flow rate on plug wall temperature

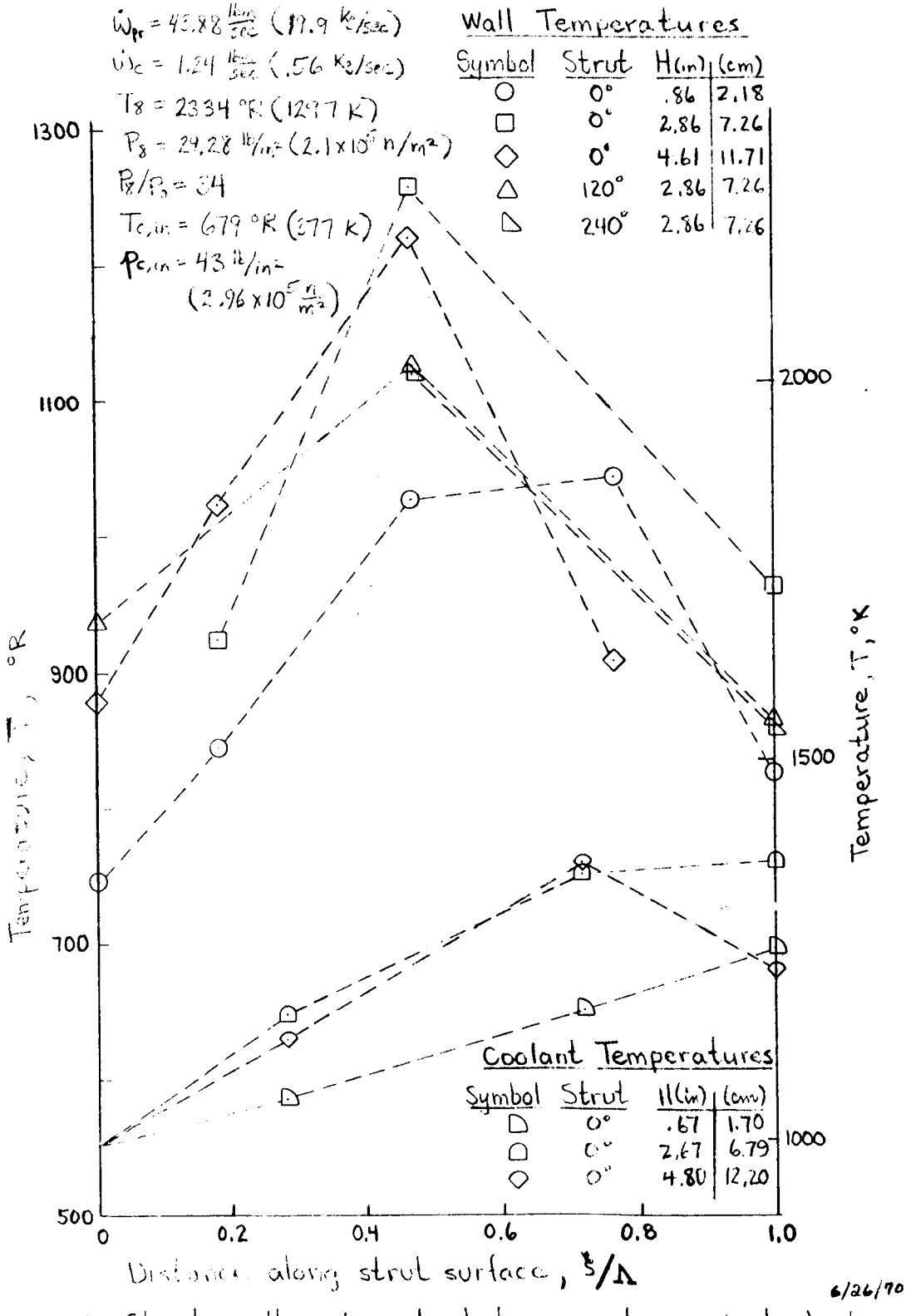

Figure 28: Strut wall and coolant temperature distributions

E-5953

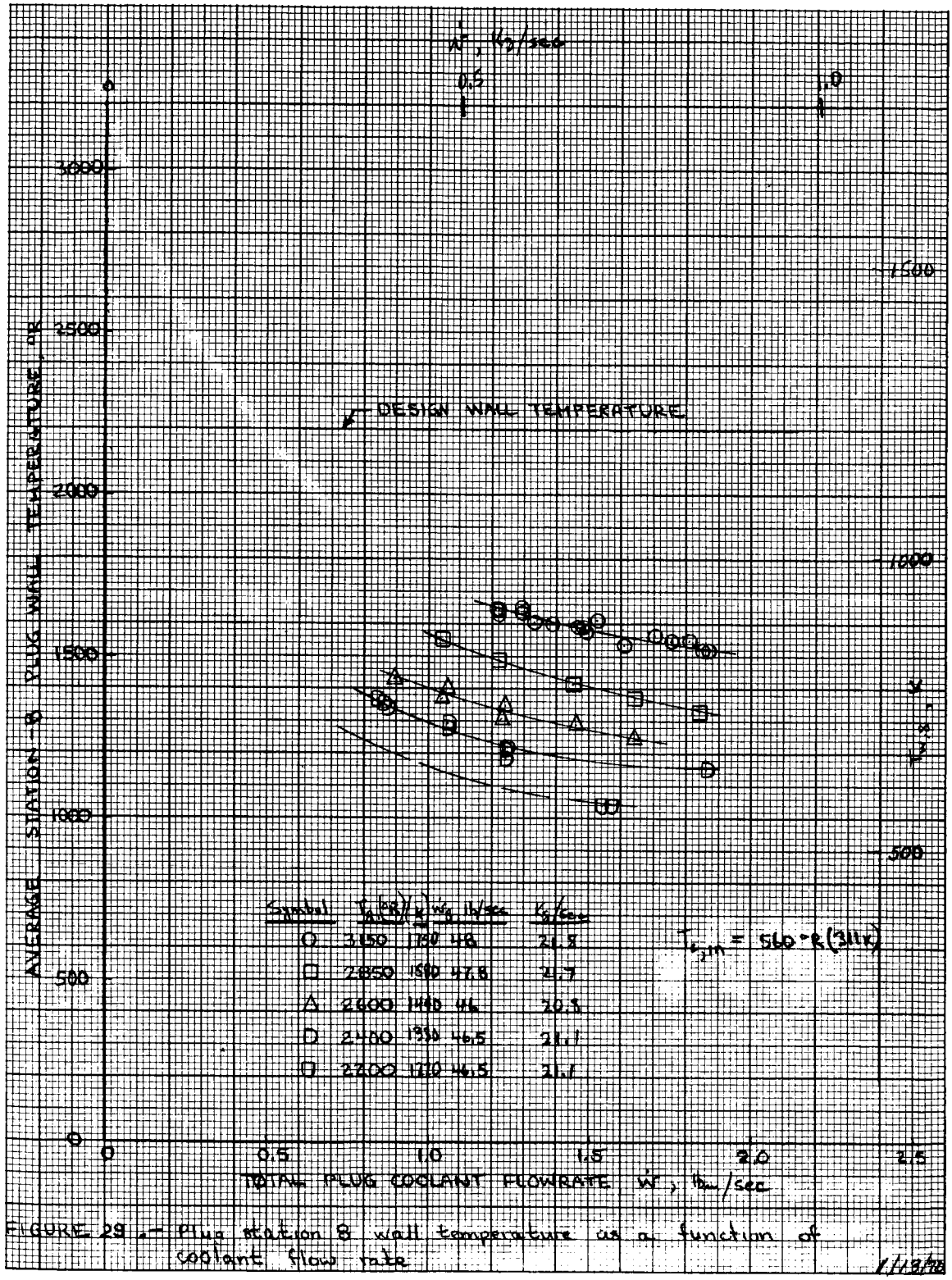

FIGURE 29. - Plug station 8 wall temperature as a function of coolant flow rate

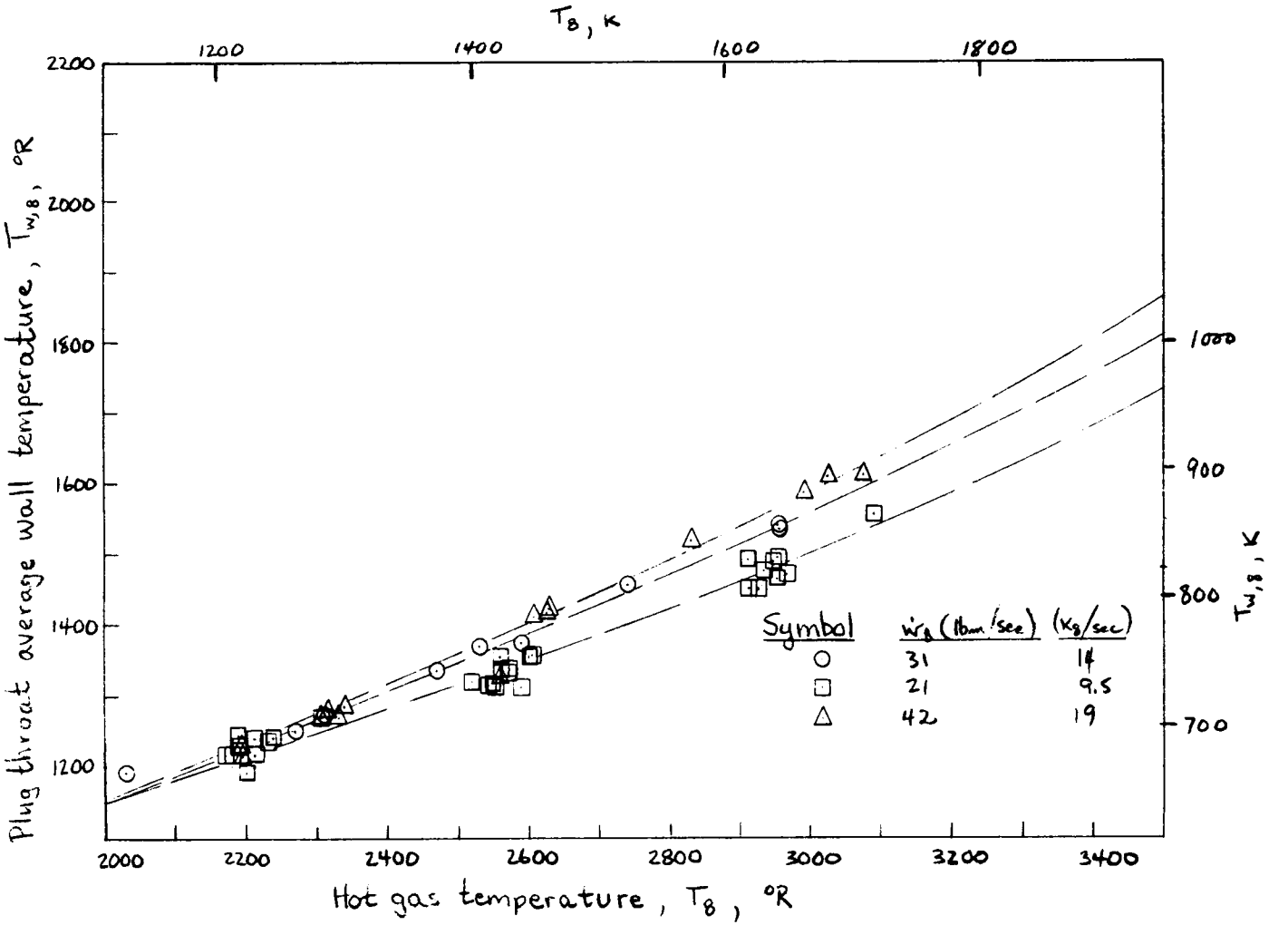

Figure 30.- Plug throat average wall temperature as a function of hot gas temperature for compressor discharge runs.

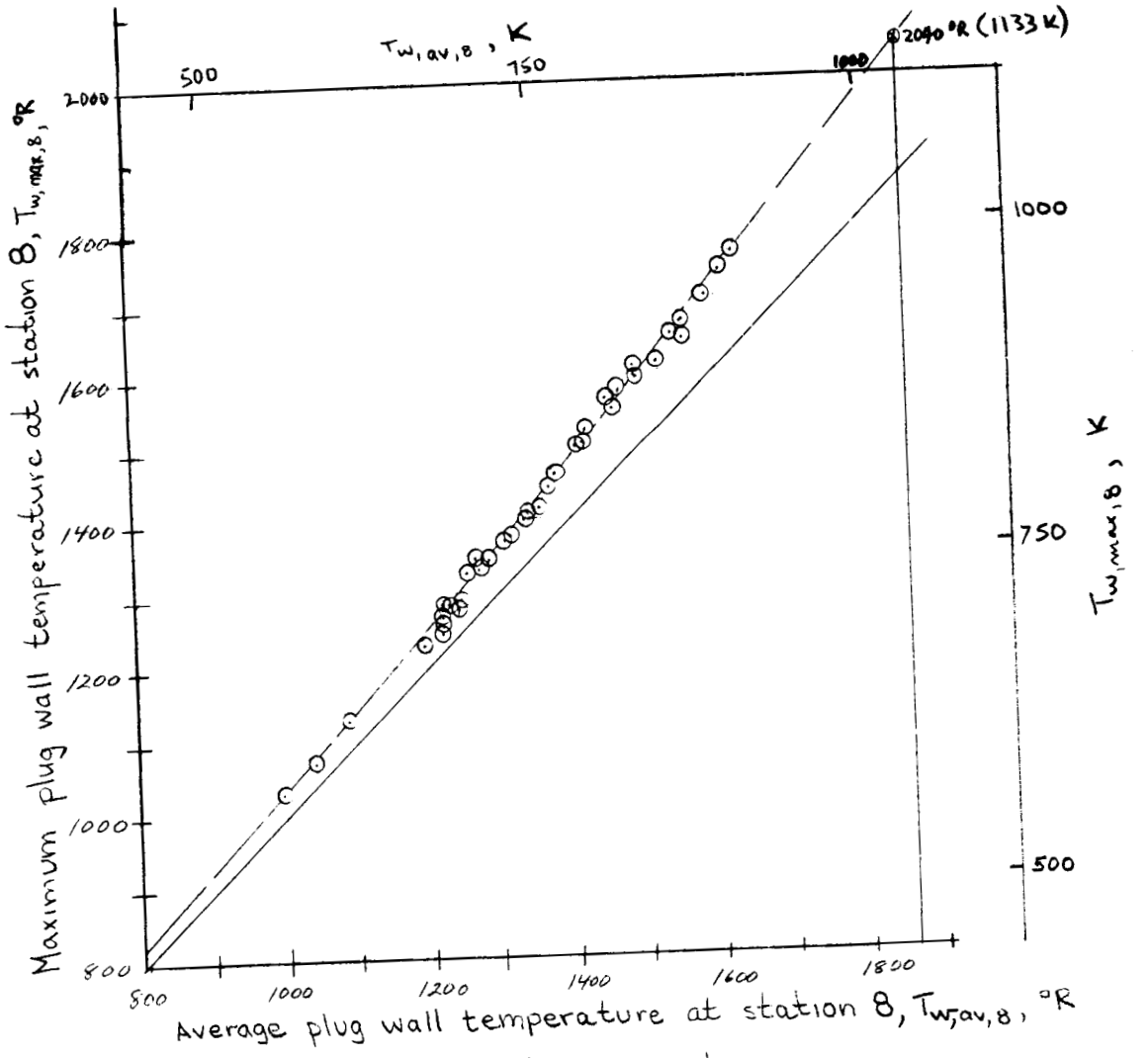

Figure 31.- Plug throat wall temperature variations.

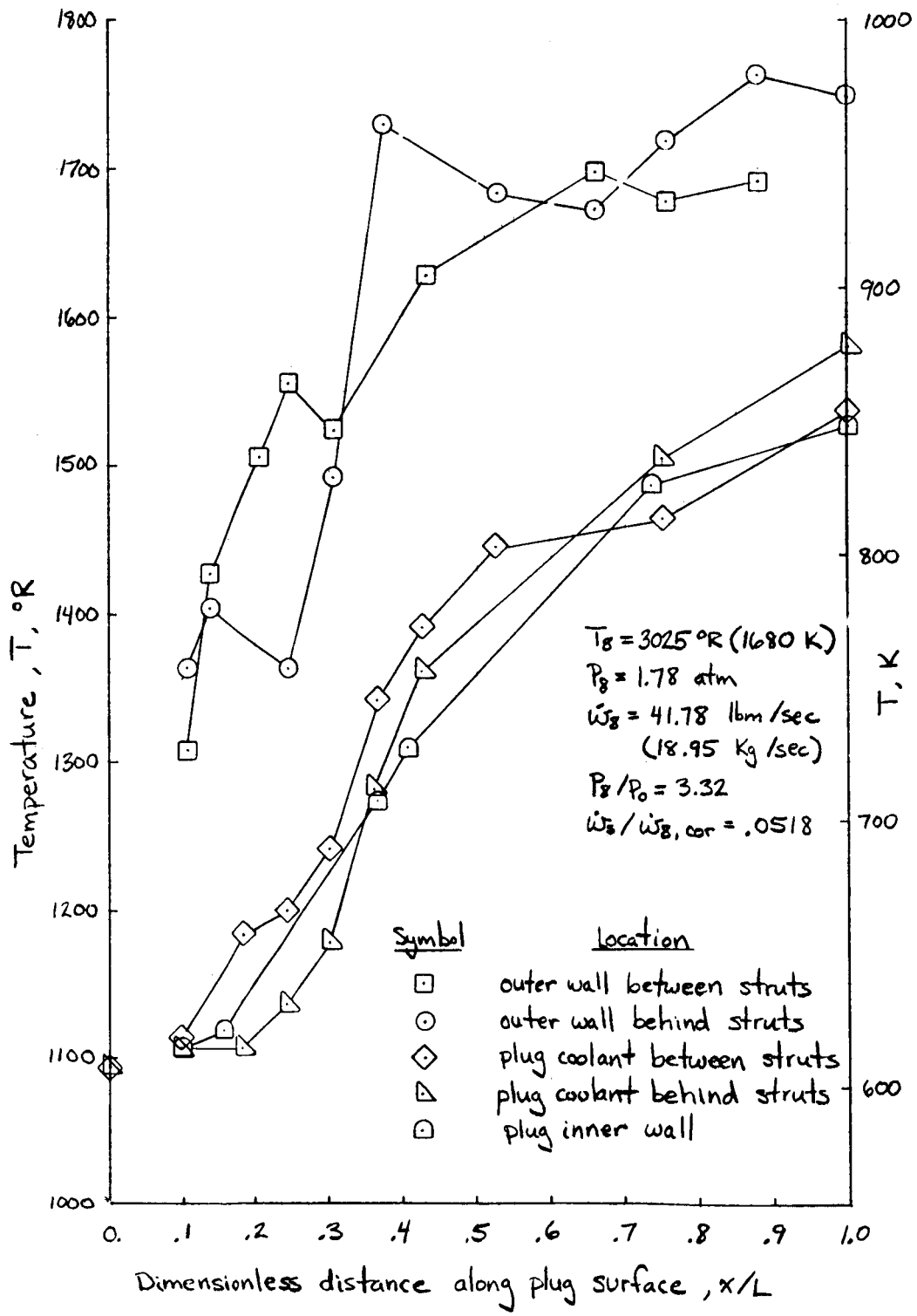

Figure 32. - Plug wall and coolant temperature distributions for simulated takeoff condition

E-5953

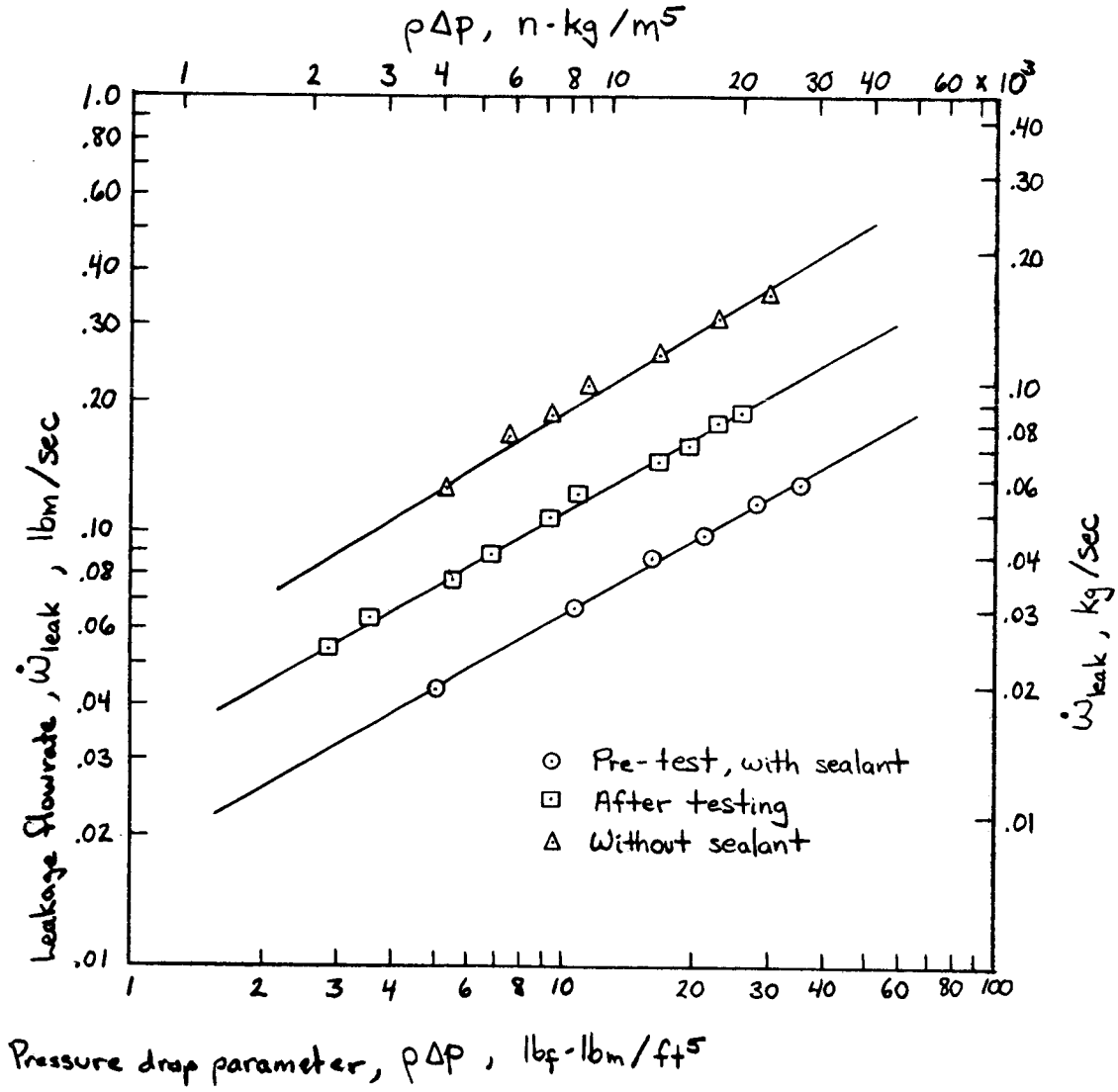

Figure 33 – Air cooled plug nozzle internal seal leakage

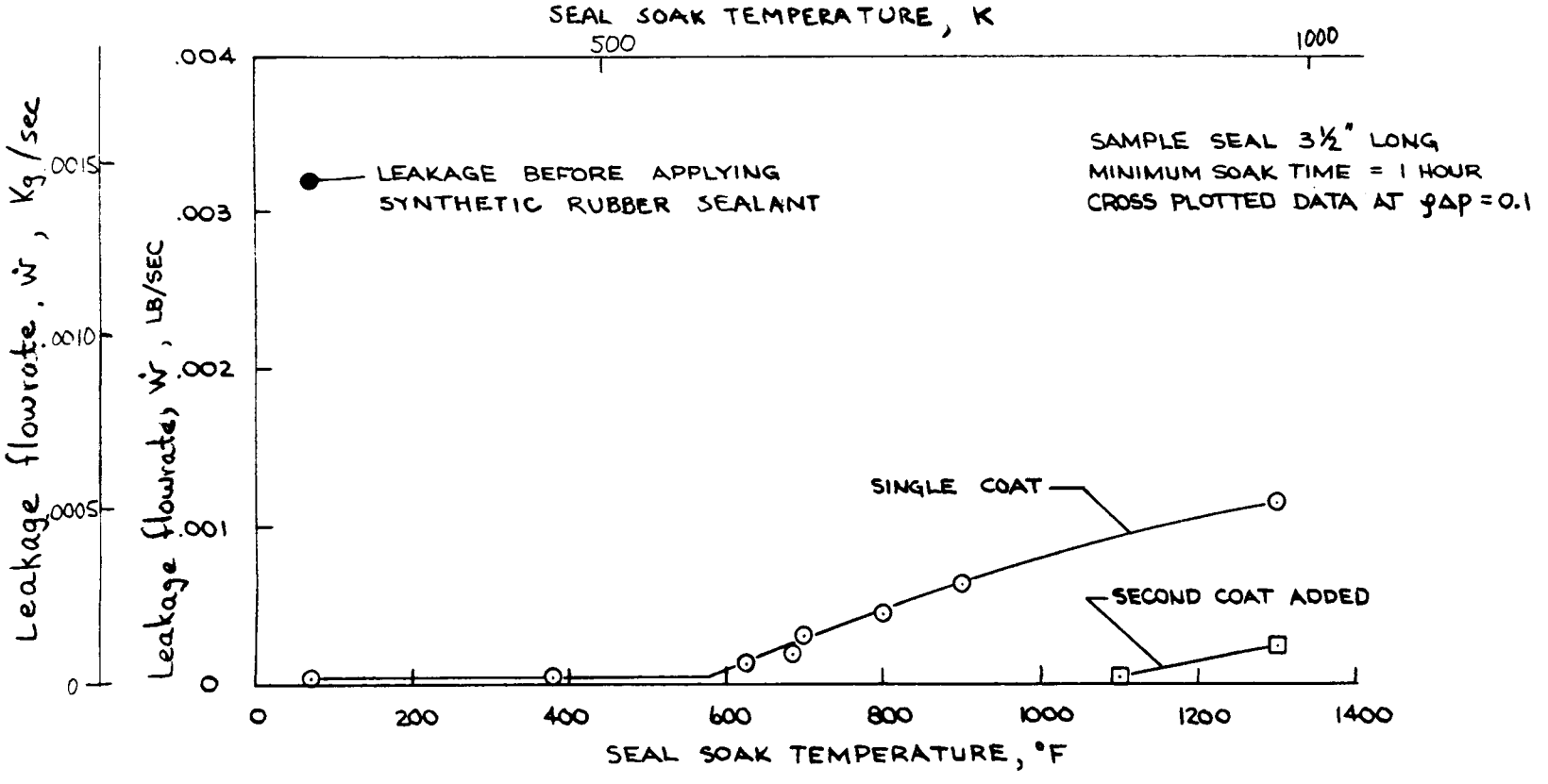

FIGURE 34.- PLUG NOZZLE SEAL SAMPLE HIGH TEMPERATURE LEAKAGE TESTS

E-5953

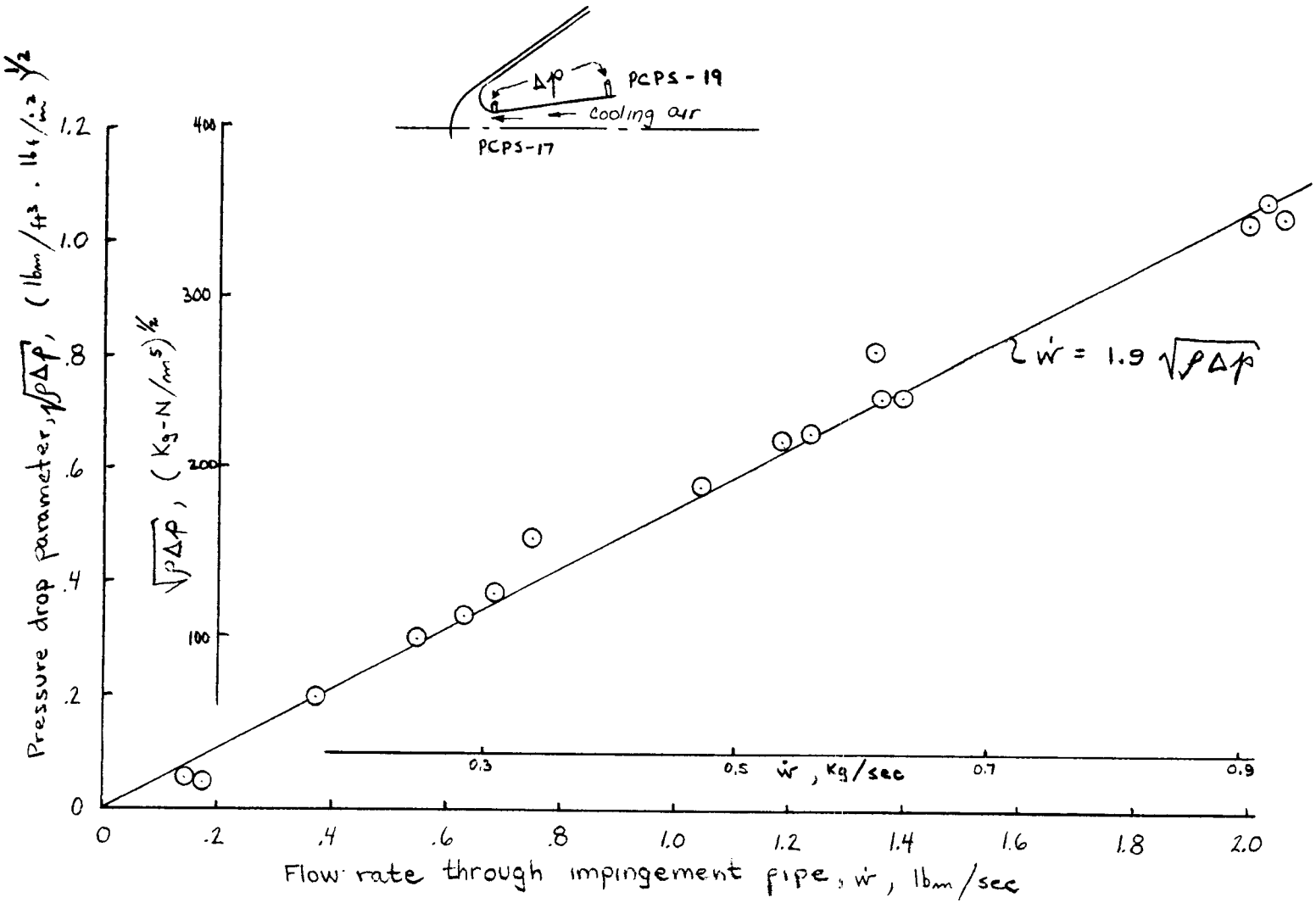

Figure 35.- Calibration of plug leading edge impingement pipe

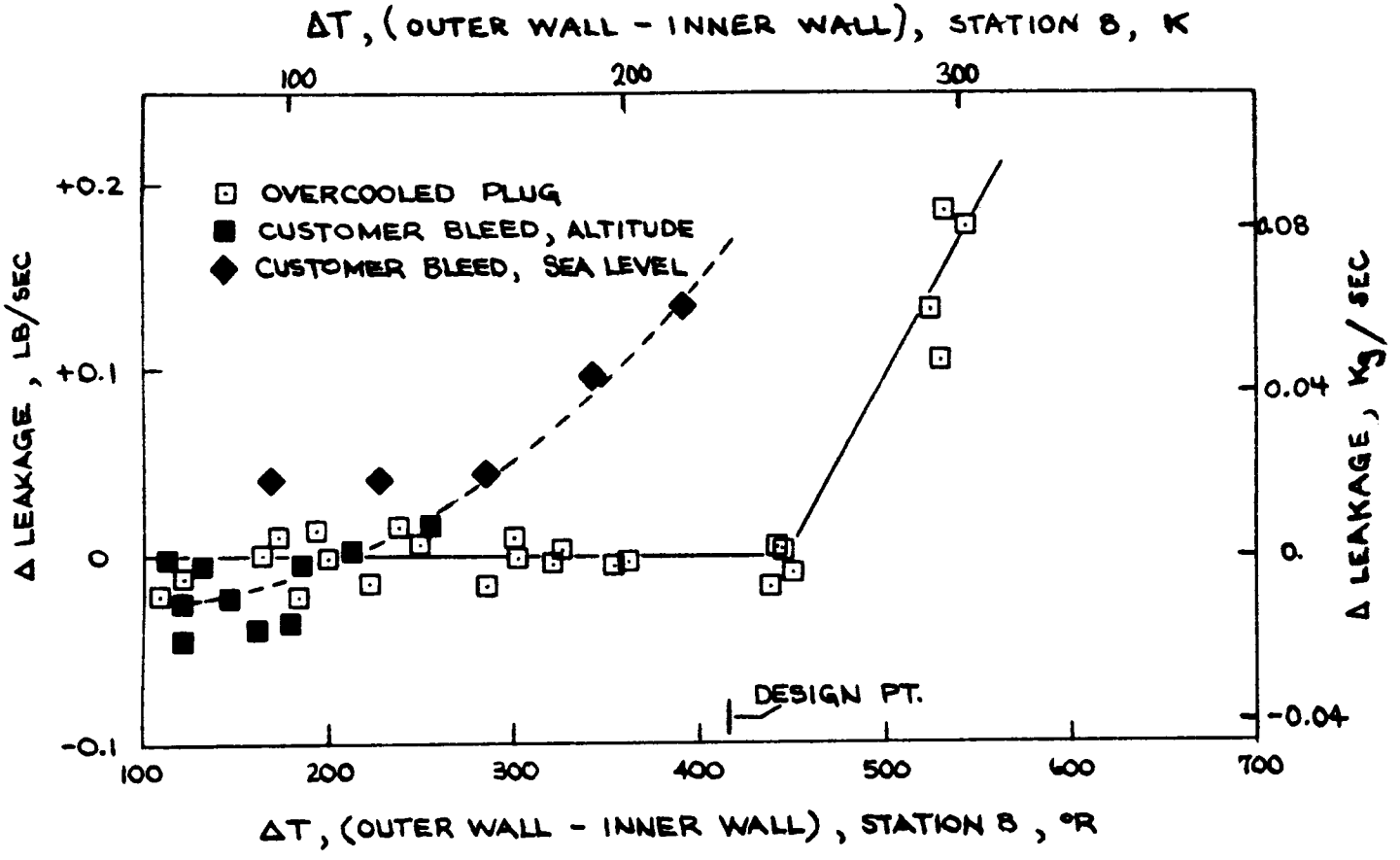

FIGURE 36 .- COOLED PLUG NOZZLE INTERNAL LEAKAGE DURING TEST PROGRAM

E-5953

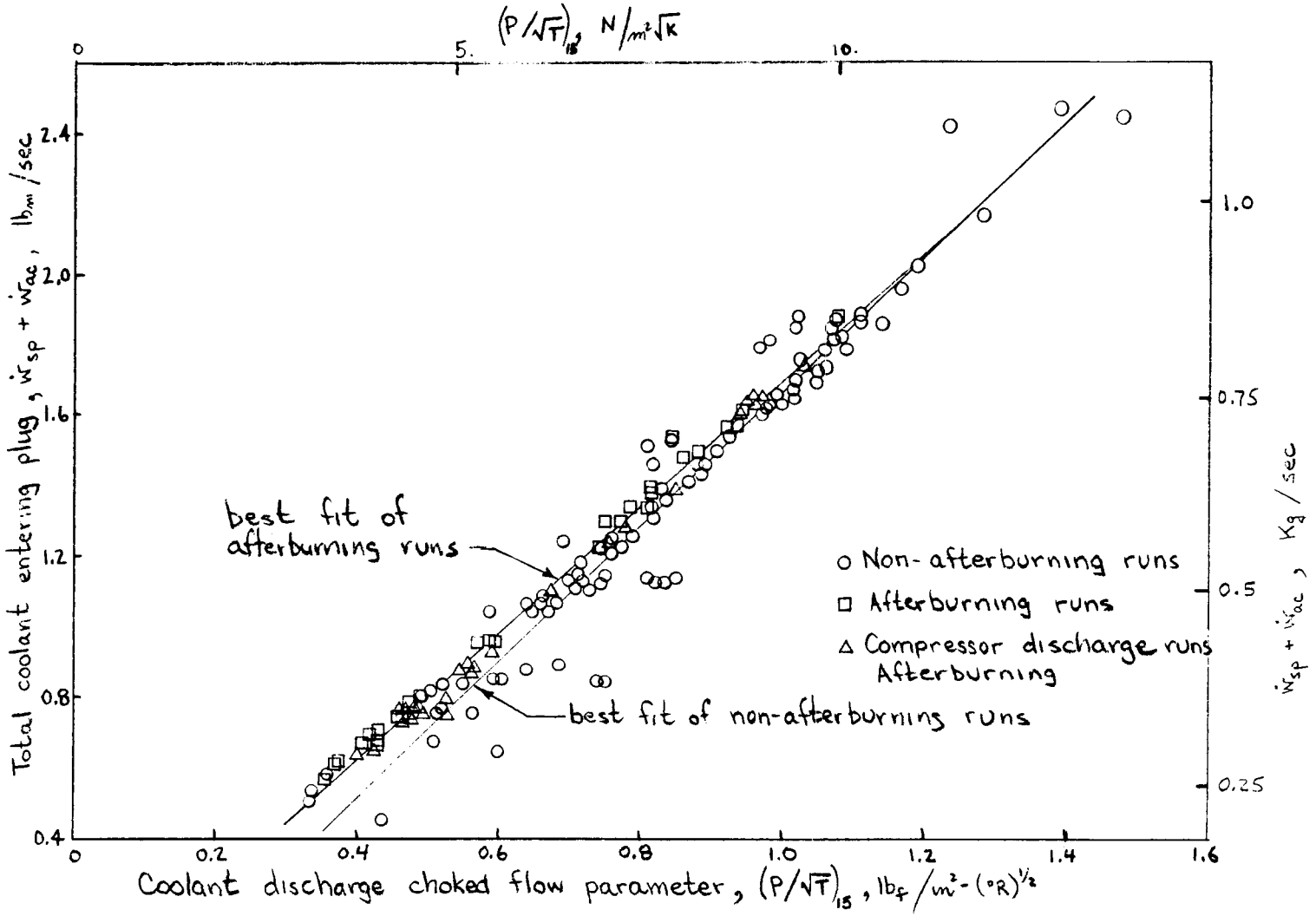

Figure 37.- Cooled plug nozzle external leakage during test program

6/23/70